

Future ocean deoxygenation driven by circulation changes: analyses of steady-state future scenarios

Benoît Pasquier¹, Mark Holzer¹,

Matthew A. Chamberlain², Richard J. Matear²,

and Nathaniel L. Bindoff³

¹School of Mathematics and Statistics, University of New South Wales, Sydney, NSW, Australia

²Commonwealth Scientific and Industrial Research Organisation, Hobart, TAS, Australia

³Australian Antarctic Program Partnership, Institute for Marine and Antarctic Studies, University of

Tasmania, Hobart, TAS, Australia

Key Points:

- Widespread deep-ocean deoxygenation is driven predominantly by a slower circulation allowing respiration to act over longer times
- Most of the reduction in preformed oxygen is driven by changes in ventilation patterns and not by warming-driven reduced solubility
- The spatial extent of upper-ocean hypoxia changes little because reduced preformed oxygen is compensated by reduced respiration

Corresponding author: Benoît Pasquier, b.pasquier@unsw.edu.au

Corresponding author: Mark Holzer, mholzer@unsw.edu.au

17 **Abstract**

18 The deoxygenation of the ocean is an important consequence of climate change that poses
19 an imminent threat to marine life and global food security. However, our understand-
20 ing of how the ocean's oxygen cycle is changing is incomplete because of the complex in-
21 teractions between changes in circulation, solubility, and respiration that drive global-
22 scale deoxygenation. Here we quantify these drivers using a data-constrained model of
23 the global marine oxygen cycle embedded in idealized steady ocean circulations for both
24 preindustrial and future perpetual 2090s conditions taken from climate-model simula-
25 tions. We disentangle the effects of the deoxygenation drivers on preformed oxygen and
26 true oxygen utilization (TOU) using the novel concept of upstream exposure time, which
27 precisely connects TOU to oxygen utilization rates and preformed oxygen to ventilation.
28 We find widespread intense deep-ocean deoxygenation due to increased TOU, driven dom-
29 inantly by a future circulation slowdown that allows respiration to act roughly 2–3 times
30 longer thereby overwhelming the effect of reduced future respiration rates. In the up-
31 per ocean, decreased respiration and slower circulation closely compensate, resulting in
32 little expansion of upper-ocean hypoxia. The bulk of preformed oxygen loss is driven by
33 ventilation shifting equatorward to where warmer surface waters hold less oxygen. Warming-
34 driven declines in solubility account for less than 10 % of the total oxygen loss. Our re-
35 sults show that the steady-state response of the oxygen cycle to changes in ocean state
36 is driven dominantly by circulation rather than by thermodynamic or biological changes.

37 **Plain Language Summary**

38 Climate change is driving oxygen out of the ocean, threatening marine life and global
39 food security. However, the precise contributions of the chemical, physical, and biolog-
40 ical processes that control oxygen levels are not well known because of their complex in-
41 teractions. Here, we address this knowledge gap by considering the long-term equilib-
42 rium of the global oxygen cycle in the idealized context of a perpetually warmer and slower
43 future ocean as if the 2090s conditions predicted by a climate model were held constant
44 in time. This allows us to quantify how much changes in solubility, respiration, and ocean
45 circulation drive ocean deoxygenation. We find strong deep-ocean deoxygenation, driven
46 by a future circulation slowdown that allows respiration to act for more than twice as
47 long overcoming lower respiration rates. The surface origin of oxygen shifts away from
48 cold high-latitude waters toward warmer waters, in which atmospheric oxygen is less sol-

49 uble, further reducing oxygen levels. Warming-driven decreases in solubility alone only
 50 account for a mere 10 % of the total oxygen loss. The upper ocean remains well oxygenated
 51 because changes in respiration and circulation compensate almost perfectly. Our results
 52 show the importance of circulation changes for controlling oxygen in the future ocean.

53 1 Introduction

54 The ocean has lost an estimated ~2 % of its oxygen content over the last 50 years
 55 (e.g., Keeling & Garcia, 2002; Whitney et al., 2007; Helm et al., 2011; Schmidtko et al.,
 56 2017; McCormick et al., 2019; Breitburg et al., 2018; Bindoff et al., 2022; Roach & Bind-
 57 off, 2023). Open-ocean deoxygenation is expected to continue in the future because of
 58 global warming, which reduces oxygen solubility and deep-ocean ventilation (e.g., Matear
 59 et al., 2000; Keeling et al., 2010; Matear & Hirst, 2003; Bopp et al., 2013; Long et al.,
 60 2019; Oschlies, 2021). There is broad consensus among models of the sixth Coupled Model
 61 Intercomparison Project (CMIP6) that hypoxic zones will expand over the next century
 62 (e.g., in the Pacific; Busecke et al., 2022) to varying degrees depending on the future emis-
 63 sions scenario (e.g., Kwiatkowski et al., 2020).

64 Ocean deoxygenation is increasingly recognized as posing an imminent threat to
 65 global marine ecosystems and food security (e.g., Earle et al., 2018; Laffoley & Baxter,
 66 2019). Oxygen is essential for life (e.g., Falkowski & Godfrey, 2008). Long-term expo-
 67 sure to sufficiently low oxygen (severe hypoxia) can be lethal to marine organisms (e.g.,
 68 Vaquer-Sunyer & Duarte, 2008; Diaz & Rosenberg, 2008). Mild to intermediate hypoxia
 69 has important physiological, behavioral, and ecological effects on marine ecosystems (e.g.,
 70 Ekau et al., 2010; Beman & Carolan, 2013; McCormick & Levin, 2017; Pascal et al., 2023;
 71 Morée et al., 2023). Hence, the distribution of oxygen in the ocean is a key control on
 72 shaping marine habitats (e.g., Rogers, 2000; Seibel, 2011; Stramma et al., 2012; Deutsch
 73 et al., 2015; Sato et al., 2017; Franco et al., 2022; Mongwe et al., under review; Deutsch
 74 et al., 2024). Even small O₂ declines and limited expansion of oxygen minimum zones
 75 (OMZs) are a major concern for global-ocean health (e.g., Gallo & Levin, 2016; Wish-
 76 ner et al., 2018; Deutsch et al., 2024).

77 Deoxygenation is driven by complex interactions among physical and biogeochem-
 78 ical processes that interact non-linearly on global scales. Oxygen in the ocean is controlled
 79 by air-sea exchange through surface winds and O₂ solubility, by photosynthetic produc-

80 tion in the surface ocean, by bacterial respiration, and by the circulation which venti-
 81 lates the ocean and connects these processes through the transport of dissolved oxygen
 82 (e.g., Oschlies et al., 2018; Levin, 2018). To attribute O₂ changes quantitatively to spe-
 83 cific driving mechanisms, a typical approach is to partition dissolved O₂ concentrations
 84 into a saturation concentration and apparent oxygen utilization (AOU; e.g., Bopp et al.,
 85 2002; Schmidtko et al., 2017; Couespel et al., 2019; Long et al., 2019; Busecke et al., 2022;
 86 Takano et al., 2023). To correct for AOU biases propagated by incomplete surface O₂
 87 saturation (Ito et al., 2004), another common approach (using models) is to compute pre-
 88 formed oxygen and “true” oxygen utilization (TOU; e.g., Oschlies et al., 2019; Palter &
 89 Trossman, 2018; Buchanan & Tagliabue, 2021; Cliff et al., 2021; Ito et al., 2022). Stud-
 90 ies based on these approaches agree qualitatively that increased oxygen utilization drives
 91 most of the deoxygenation, with reduced solubility accounting for less than 50 % of upper-
 92 ocean deoxygenation, and less than ~25 % of the deoxygenation of the entire water col-
 93 umn. However, how much of the AOU (or TOU) increase can be attributed to changes
 94 in ventilation (i.e., circulation) versus respiration remains unclear (e.g., Breitburg et al.,
 95 2018; Oschlies et al., 2018).

96 While the importance of circulation for open-ocean hypoxia was recognized long
 97 ago (e.g., Wyrtki, 1962; Sarmiento et al., 1988), its precise contribution to changes in
 98 preformed O₂ and oxygen utilization has yet to be quantified (Oschlies et al., 2018). This
 99 is a challenging task because disentangling the effects of circulation changes from the ef-
 100 fects of changes in solubility and upstream respiration requires a careful accounting of
 101 all possible oxygen pathways and losses. To avoid these difficulties, some studies resort
 102 to perturbation experiments, under the tacit assumption that the system is sufficiently
 103 linear to infer the thermal and physical contributions to deoxygenation from the differ-
 104 ence between perturbed and unperturbed simulations. These perturbed simulations may
 105 consist, for example, in keeping surface solubility fixed in time (e.g., Matear et al., 2000;
 106 Matear & Hirst, 2003; Couespel et al., 2019), in keeping oxygen utilization rates (OUR)
 107 fixed in time (e.g., Deutsch et al., 2006), in removing biogeochemical processes (e.g., Cliff
 108 et al., 2021), or in a combination of the above (e.g., Plattner et al., 2001; Bopp et al.,
 109 2002). To assess circulation control on oxygen loss, other perturbations consist in keep-
 110 ing the circulation fixed in its preindustrial state (e.g., Palter & Trossman, 2018). Such
 111 residual-based perturbation approaches can be strongly biased by spatial correlations be-
 112 tween changes in solubility and changes in circulation that are typically ignored. How-

ever, as we show here, such correlations can be of first order for large perturbations or over long timescales. Also commonly used for assessing the effects of circulation changes on deoxygenation is the ideal mean age, often invoked as an empirical timescale linking TOU and OUR (e.g., Bopp et al., 2017; Palter & Trossman, 2018; Busecke et al., 2022). However, all the studies mentioned here ultimately fall short of accurately attributing deoxygenation to its drivers because they lack a quantitative framework, based on the underlying fundamental equations, that connects TOU to OUR with the correct circulation timescale.

Here, we rigorously partition O_2 changes into contributions from circulation changes, solubility changes, and their spatial correlations by employing the exact timescale that connects TOU to upstream OUR. Specifically, in steady state, the local OUR contribution at location \mathbf{r} to the TOU content of an interior volume Ω has recently been shown to be $OUR(\mathbf{r}) \times \Gamma_\Omega^\uparrow(\mathbf{r})$, where $\Gamma_\Omega^\uparrow(\mathbf{r})$ is the “upstream exposure time”, i.e., the time that the water in Ω spent sweeping past upstream location \mathbf{r} , and hence the time over which $OUR(\mathbf{r})$ acts (Holzer, 2022). Importantly, Γ_Ω^\uparrow is a fundamental timescale of the circulation only. Furthermore, we show here that Γ_Ω^\uparrow also connects the preformed O_2 content of Ω to its surface origin.

We focus here on idealized steady states to probe the oxygen cycle on all its fundamental timescales, including the very long timescales that cannot be explored with typical centennial-scale transient simulations. In addition, steady state affords many computational advantages that we exploit extensively. For the reference state, we use preindustrial conditions and for the future we use decadal-mean circulations of the 2090s, all as simulated by the Australian Community Climate and Earth System Simulator (ACCESS1.3 Bi et al., 2013). We hold the 2090s circulations fixed in time for perpetuity, embed the intermediate-complexity PCO₂ biogeochemistry model (Pasquier, Holzer, Chamberlain, Matear, et al., 2023) and solve for steady state using a Newton method.

We find intense global-scale deoxygenation in the steady future states. The future oxygen distribution is characterized by widespread expansion of mild to severe hypoxia, predominantly at depth. In the upper ocean, hypoxic regions do not expand appreciably because decreases in preformed oxygen are compensated by colocated TOU reductions, driven primarily by reduced respiration rates. In the deep ocean, by contrast, strong increases in TOU are predominantly driven by the slower future circulation allowing res-

145piration to act over 2 to 3 times longer. Preformed oxygen declines almost everywhere,
 146 driven primarily by equatorward shifts in ventilation, with reduced solubility only play-
 147 ing a secondary role (order 10 % of the total oxygen loss). Our analyses highlight the over-
 148 arching importance of the circulation in determining the ocean’s oxygen content through
 149 its control on ventilation patterns and the path-integrated oxygen utilization.

150 **2 Methods**

151 **2.1 Preindustrial and future ocean circulation**

152 We consider a preindustrial and two idealized future ocean states that are steady,
 153 i.e., frozen in time. Specifically, we use simulations from the Australian Community Cli-
 154 mate and Earth System Simulator (ACCESS1.3; Marsland et al., 2013; Bi et al., 2013),
 155 and average their ocean circulation and thermodynamic state variables (including tem-
 156 perature and salinity). A 1990s decadal average is used as an approximately preindus-
 157 trial state, and a 2090s decadal average is used to represent future states corresponding
 158 to an intermediate and a worst-case climate-change scenario (Representative Concen-
 159 tration Pathways RCP4.5 and RCP8.5; Meinshausen et al., 2011, 2020). For further de-
 160 tails, see the work of Pasquier, Holzer, and Chamberlain (2023) who used the same steady-
 161 state framework for quantifying the drivers of changes in the ocean’s carbon pumps.

162 The advective–diffusive flux-divergence operator of each state is organized into a
 163 sparse transport matrix following Chamberlain et al. (2019). The model grid employed
 164 (coarse-grained from the original ACCESS1.3 grid) has a nominal horizontal resolution
 165 of $2^\circ \times 2^\circ$ (finer in the tropics) and 50 vertical levels with thicknesses increasing from 10 m
 166 at the surface to 335 m at depth. While ACCESS1.3 is a state-of-the-art climate model,
 167 when interpreting results below it is important to note that its preindustrial circulation
 168 features an unrealistically deep mixed layer near the Weddell and Ross Seas (with MLDs
 169 reaching below 5000 m; see, e.g., Bi et al., 2013) that strongly shoals in the future, with
 170 substantial effects on our future steady states (as in Pasquier, Holzer, & Chamberlain,
 171 2023). Although deep ventilation through convection is unrealistic (e.g., Heuzé et al.,
 172 2013), the model’s decline in deep Southern Ocean ventilation driven by climate change
 173 is consistent with recent observations: Antarctic Bottom Water formation has been ob-
 174 served to decline in recent decades and is predicted to decline strongly over the next few
 175 decades (e.g., de Lavergne et al., 2014; Gunn et al., 2023; Li et al., 2023).

176 **2.2 Oxygen cycle model**

177 For the oxygen cycle, we use the PCO₂ biogeochemistry model of Pasquier, Holzer,
 178 Chamberlain, Matear, et al. (2023). PCO₂ is embedded in the steady ocean circulations
 179 using our transport matrices, and we solve directly for the biogeochemical steady state
 180 using a Newton Method. Our future steady-state oxygen cycles thus correspond to the
 181 equilibrium that would ultimately be reached if the thermodynamic and physical state
 182 of the ocean were held at its 2090s level in perpetuity.

183 A key feature of PCO₂ for capturing the response of dissolved oxygen to climate
 184 change is that PCO₂ explicitly models the nonlinear interactions and feedbacks between
 185 oxygen, carbon, and nutrients. This includes the effects of oxygen and particulate or-
 186 ganic matter on respiration, and the effects of temperature on biological production and
 187 respiration. The biogeochemical parameters of PCO₂ were objectively optimized for prein-
 188 dustrial conditions against observations of phosphate, dissolved inorganic carbon, total
 189 alkalinity, and oxygen. Oxygen in the optimized state has a global volume-weighted root-
 190 mean-square model–observations mismatch of $\sim 30 \mu\text{M}$ (Pasquier, Holzer, Chamberlain,
 191 Matear, et al., 2023). Systematic biases, in part inherited from the parent ACCESS-model
 192 circulation, remain despite parameter optimization, with underestimated O₂ in the up-
 193 per tropical Pacific and Atlantic above $\sim 1000 \text{ m}$ and overestimated O₂ in the Southern
 194 Ocean and the tropical Indian Ocean (see Appendix Fig. A1 for a comparison between
 195 modelled and observed zonal mean $p\text{O}_2$). However, we deem these biases acceptable as
 196 they are smaller than for most CMIP5 models (Bao & Li, 2016) and because they are
 197 generally dwarfed by the much larger future changes analyzed here.

198 In the PCO₂ model, oxygen enters and exits the ocean through air–sea gas exchange,
 199 is photosynthetically produced in the euphotic layer, and is utilized through aerobic bac-
 200 terial respiration. In steady state, the three-dimensional O₂ concentrations obeys

$$201 \quad \mathcal{T} \text{O}_2 = P - \text{OUR} + J_{\text{atm}}, \quad (1)$$

202 where $\mathcal{T} \text{O}_2$ is the advective–diffusive flux divergence of dissolved oxygen, $P = r_{\text{O}_2:\text{C}} U_{\text{C}}$
 203 is the photosynthetic production of oxygen keyed to biological carbon uptake U_{C} through
 204 the optimized $r_{\text{O}_2:\text{C}} = 1.31 \text{ molO}_2 \text{ molC}^{-1}$, and $\text{OUR} = r_{\text{O}_2:\text{C}} (R_{\text{DOC}} + R_{\text{POC}}) \Theta(\text{O}_2 -$
 205 $\text{O}_2^{\text{lim}})$ is the oxygen utilization rate keyed to respiration of dissolved and particulate or-
 206 ganic carbon (R_{DOC} and R_{POC}). (The Θ term switches off aerobic respiration when O₂
 207 drops below $\text{O}_2^{\text{lim}} = 5 \mu\text{M}$, implicitly representing the effect of anaerobic denitrification.)

Air-sea gas exchange is modelled using the parameterization $J_{\text{atm}} = k (K_0 pO_2^{\text{atm}} - O_2)/h$ at the surface (Wanninkhof, 2014), where k is the wind- and temperature-dependent gas-transfer velocity, K_0 is the temperature- and salinity-dependent oxygen solubility, pO_2^{atm} is the oxygen atmospheric partial pressure (based on an atmospheric oxygen mixing ratio of 0.210 for both preindustrial and future states), and $h = 10 \text{ m}$ is the thickness of the top model layer.

2.3 Preformed oxygen, O_2^{pre}

Preformed oxygen is defined here as the oxygen that would be propagated by the ocean circulation out of the euphotic-layer and into the ocean's interior in the absence of any aphotic sources and sinks. Hence, O_2^{pre} depends only on euphotic O_2 concentrations and on ventilation patterns (see Appendix B for details on how O_2^{pre} is computed).

To separate the effects of solubility from the effects of circulation on O_2 within the euphotic zone, we further decompose O_2^{pre} into a saturated component O_2^{sat} and a disequilibrium component $O_2^{\text{dis}} = O_2^{\text{pre}} - O_2^{\text{sat}}$. This decomposition is useful because the air-sea O_2 disequilibrium varies with location and can be important in deep-water formation regions (see, e.g., Russell & Dickson, 2003; Ito et al., 2004; Duteil et al., 2013; Eggleston & Galbraith, 2018).

2.4 True oxygen utilization, TOU

To quantify the oxygen deficit caused by loss to respiration, we use “true oxygen utilization” $\text{TOU} = O_2^{\text{pre}} - O_2$ (e.g., Broecker & Peng, 1982; Ito et al., 2004; Koeve & Kähler, 2016; Holzer, 2022). TOU is thus the cumulated amount of oxygen that has been removed by respiration along its interior transit since leaving the euphotic zone (computational details in Appendix B). Note that $-\text{TOU}$ may also be thought of as regenerated oxygen, $O_2 - O_2^{\text{pre}}$ (e.g., DeVries & Deutsch, 2014).

2.5 Deoxygenation drivers

To summarize the contributions from changes in circulation, solubility, or respiration, it is useful to integrate the oxygen change over a specific subvolume Ω of interest. We will first consider TOU and then O_2^{pre} .

236 **2.5.1 Change in TOU**

The Ω inventory of TOU is controlled at every location \mathbf{r} upstream of Ω by $\text{OUR}(\mathbf{r})$ and by the time that the water currently in Ω spent flowing past \mathbf{r} , which is the time for which $\text{OUR}(\mathbf{r})$ acts on the oxygen heading toward Ω . This timescale, which we call “upstream exposure time” here, was only recently computed by Holzer (2022), who showed that for steady flow it is equal to $\Gamma_\Omega^\uparrow(\mathbf{r})$, the mean time that water currently at \mathbf{r} will spend in Ω on its way to the surface. In steady state, $\Gamma_\Omega^\uparrow(\mathbf{r})$ equals the time that oxygen at \mathbf{r} was exposed to respiration upstream of Ω and connects the TOU inventory to $\text{OUR}(\mathbf{r})$ through the relationship (Holzer, 2022):

$$\int_{\Omega} \text{TOU}(\mathbf{r}) d^3\mathbf{r} = \int \text{OUR}(\mathbf{r}) \Gamma_\Omega^\uparrow(\mathbf{r}) d^3\mathbf{r}. \quad (2)$$

The integrals in Eq. (2) are easily computed in matrix form (Appendix B). We emphasize that the upstream exposure time (Γ_Ω^\uparrow in steady state) is fundamentally different from the ideal mean age (e.g., Primeau, 2005), which is commonly used to approximately relate TOU or AOU to OUR (e.g., Doney & Bullister, 1992; Warner et al., 1996; Zheng et al., 1997; Feely et al., 2004; Bopp et al., 2017; Palter & Trossman, 2018, to cite a few), despite known systematic biases (e.g., Duteil et al., 2013; Sonnerup et al., 2013; Brandt et al., 2015; Sonnerup et al., 2015; Koeve & Kähler, 2016; Thomas et al., 2020).

The quantitative connection of TOU with OUR through Γ_Ω^\uparrow in Eq. (2) allows us to partition TOU changes into contributions from changes in respiration, circulation, and their interaction. Specifically, we algebraically decompose, at every point \mathbf{r} of the ocean, the change in the integrand ($\text{OUR} \times \Gamma_\Omega^\uparrow$) on the right-hand-side of Eq. (2) as

$$\Delta(\text{OUR} \times \Gamma_\Omega^\uparrow) = \underbrace{\Gamma_\Omega^\uparrow \Delta\text{OUR}}_{\text{respiration}} + \underbrace{\text{OUR} \Delta\Gamma_\Omega^\uparrow}_{\text{circulation}} + \underbrace{\Delta\text{OUR} \Delta\Gamma_\Omega^\uparrow}_{\text{cross term}}, \quad (3)$$

where a quantity X not preceded by Δ denotes its preindustrial value and $\Delta X = X_{\text{future}} - X$ is the future change in X . The driving process represented by each term is indicated beneath the braces of Eq. (3), and these terms are globally integrated to give the corresponding contributions to the changes in the Ω inventory of TOU in accord with Eq. (2). The $\Gamma_\Omega^\uparrow \Delta\text{OUR}$ term corresponds to the contribution from respiration-only changes, with the circulation fixed at its preindustrial state, while $\text{OUR} \Delta\Gamma_\Omega^\uparrow$ corresponds to the contribution from circulation-only changes, with OUR fixed at its preindustrial value, and the “cross term” $\Delta\text{OUR} \Delta\Gamma_\Omega^\uparrow$ corresponds to the simultaneous colocated changes in OUR and upstream exposure time. To the best of our knowledge, this is the first decompo-

267 sition to cleanly separate respiration-only and circulation-only effects, and to explicitly
 268 account for the effect of simultaneous changes in both respiration and circulation.

269 **2.5.2 Change in O_2^{pre}**

270 In steady state, the Ω inventory of preformed oxygen is determined by euphotic oxy-
 271 gen concentrations modulated by the amount of Ω -volume ventilated per unit area at
 272 the base of the euphotic zone, $\mathcal{V}_\Omega^\downarrow$. Mathematically,

$$273 \int_\Omega O_2^{\text{pre}}(\mathbf{r}) d^3\mathbf{r} = \int O_2(\mathbf{r}_s) \mathcal{V}_\Omega^\downarrow(\mathbf{r}_s) d^2\mathbf{r}_s, \quad (4)$$

274 where location \mathbf{r}_s ranges over the base of the euphotic layer. (A derivation together with
 275 computational details is given in Appendix B.) The Ω volume ventilated per unit area
 276 $\mathcal{V}_\Omega^\downarrow$ is a generalization of the ocean volume ventilated per unit area (e.g., Primeau, 2005;
 277 Holzer et al., 2020). (We note in passing that $\mathcal{V}_\Omega^\downarrow$ is also proportional to the volume frac-
 278 tions f_{ij} derived by Fu et al. (2018) for quantifying the ventilation of OMZs, through
 279 $f_{ij} = A_{ij} \mathcal{V}_\Omega^\downarrow / v_\Omega$, where A_{ij} is the surface grid cell area and v_Ω is the Ω volume.) What
 280 is new and important here is the quantitative connection between the Ω inventory of O_2^{pre}
 281 and euphotic O_2 concentrations provided by $\mathcal{V}_\Omega^\downarrow$. In Appendix B we furthermore provide
 282 a new relation between $\mathcal{V}_\Omega^\downarrow$ and Γ_Ω^\uparrow , with $\mathcal{V}_\Omega^\downarrow$ being the flux of Γ_Ω^\uparrow into the euphotic zone
 283 because Γ_Ω^\uparrow traces the O_2^{pre} currently in Ω back to its euphotic origin.

284 Similar to our analysis of TOU changes, we partition changes in the Ω inventory
 285 of O_2^{pre} into contributions from changes in solubility and circulation. To this end, we al-
 286 gebraically decompose, at every point \mathbf{r}_s at the base of the euphotic layer, the change
 287 in the integrand $O_2 \mathcal{V}_\Omega^\downarrow$ on the right-hand-side of Eq. (4) as

$$288 \Delta(O_2 \mathcal{V}_\Omega^\downarrow) = \underbrace{\mathcal{V}_\Omega^\downarrow \Delta O_2^{\text{sat}}}_{\text{solubility}} + \underbrace{O_2^{\text{sat}} \Delta \mathcal{V}_\Omega^\downarrow}_{\text{circulation}} + \underbrace{\Delta(O_2^{\text{dis}} \mathcal{V}_\Omega^\downarrow)}_{\text{cross term}}, \quad (5)$$

289 where we have further separated euphotic O_2 into its saturated and disequilibrium com-
 290 ponents and the driving process represented by each term is indicated beneath the braces.
 291 The term $\mathcal{V}_\Omega^\downarrow \Delta O_2^{\text{sat}}$ accounts for the contribution to ΔO_2^{pre} in Ω from solubility-only changes
 292 by keeping the circulation (and thus ventilation volumes $\mathcal{V}_\Omega^\downarrow$) fixed in its preindustrial
 293 state. The contribution from circulation-only changes includes $O_2^{\text{sat}} \Delta \mathcal{V}_\Omega^\downarrow$, where surface
 294 solubility is fixed at its preindustrial values, and $\Delta(O_2^{\text{dis}} \mathcal{V}_\Omega^\downarrow)$, which we consider to be
 295 a circulation-only effect by assuming that O_2^{dis} is entirely driven by circulation changes.
 296 The decomposition of Eq. (5) is, to the best of our knowledge, also new.

297 **2.6 Hypoxia severity categories**

298 To quantify the extent of low-oxygen conditions, we follow Hofmann et al. (2011)
 299 and define hypoxia categories A, B, and C, ranging from mild to severe in terms of the
 300 in situ effective partial pressure of oxygen, pO_2 . Specifically for our model, category-A
 301 mild hypoxia is deemed to occur where $pO_2 \leq 100$ matm, category-B intermediate hy-
 302 poxia where $pO_2 \leq 50$ matm, and category-C severe hypoxia where $pO_2 \leq 15$ matm.
 303 Note that we have adjusted the $pO_2 = 106, 60$, and 22 matm thresholds of Hofmann
 304 et al. (2011) such that the modelled global hypoxia volume for each category matches
 305 the values based on GLODAPv2 observations (Lauvset et al., 2016). Despite matching
 306 the global hypoxic volumes, the horizontal extent of hypoxic regions remain overestimated
 307 in the Pacific and Atlantic and underestimated in the Indian Ocean (see Appendix Figs. A2
 308 and A3 for more details).

309 **3 Results**310 **3.1 Global deoxygenation and expansion of hypoxic regions**

311 We find intense deoxygenation for our steady future states, with the global oxy-
 312 gen inventory decreasing by 30 % and 60 % for the RCP4.5- and RCP8.5-based states,
 313 respectively. Figure 1 shows the basin zonal-mean pO_2 for each scenario and the corre-
 314 sponding preindustrial-to-future change. (We show the effective partial pressure, pO_2 ,
 315 because it is the most relevant thermodynamic oxygen quantity for critical physiolog-
 316 ical processes in living organisms (Hofmann et al., 2011).) The oxygen loss is largest in
 317 the Pacific because of the dramatically reduced ventilation from Antarctic Bottom Wa-
 318 ter (AABW). Oxygen loss is also intense in the Atlantic sector of the Southern Ocean,
 319 but deoxygenation in the Atlantic is overall less pronounced as the mid-depth North At-
 320 lantic remains ventilated by North Atlantic Deep Water (NADW) in the future. Deoxy-
 321 genation does not occur everywhere however, with slight increases in the zonal mean pO_2
 322 occurring close to the surface in each basin, particularly at northern mid-latitudes in the
 323 Atlantic and Indian Ocean (Fig. 1j–o), likely due to reduced local respiration and shoal-
 324 ing NADW.

325 The expansion of hypoxic zones depends strongly on the severity (i.e., pO_2 thresh-
 326 old) of hypoxia considered, on the local ventilation, and on the climate-change scenario.
 327 Figure 2 shows the profiles of the spatial extent of each hypoxia category (Methods, Sec-

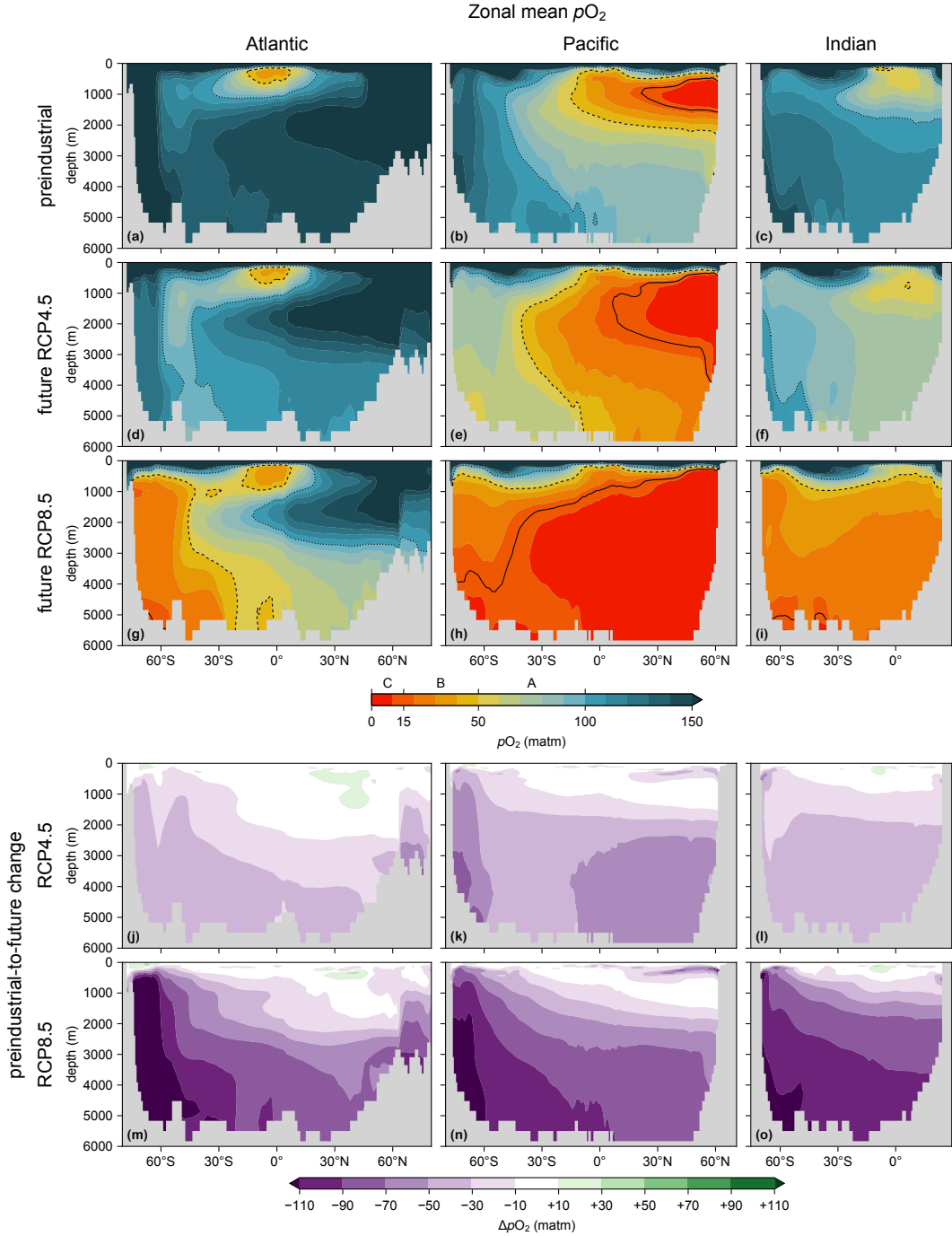


Figure 1. (a) Atlantic, (b) Pacific, and (c) Indian Ocean zonal mean $p\text{O}_2$ for the preindustrial state. The dotted, dashed, and solid contour lines indicate the $p\text{O}_2 = 100, 50, 15 \text{ matm}$ thresholds of hypoxia categories A, B, and C, respectively. (d–f) As (a–c) for the future RCP4.5-based state. (g–i) As (d–f) for RCP8.5. (j–o) As (d–i) for the preindustrial-to-future change. The Atlantic basin excludes the Gulf of Mexico and the Caribbean, and the Pacific basin excludes the Sea of Japan so that the zonal means are more cleanly interpretable.

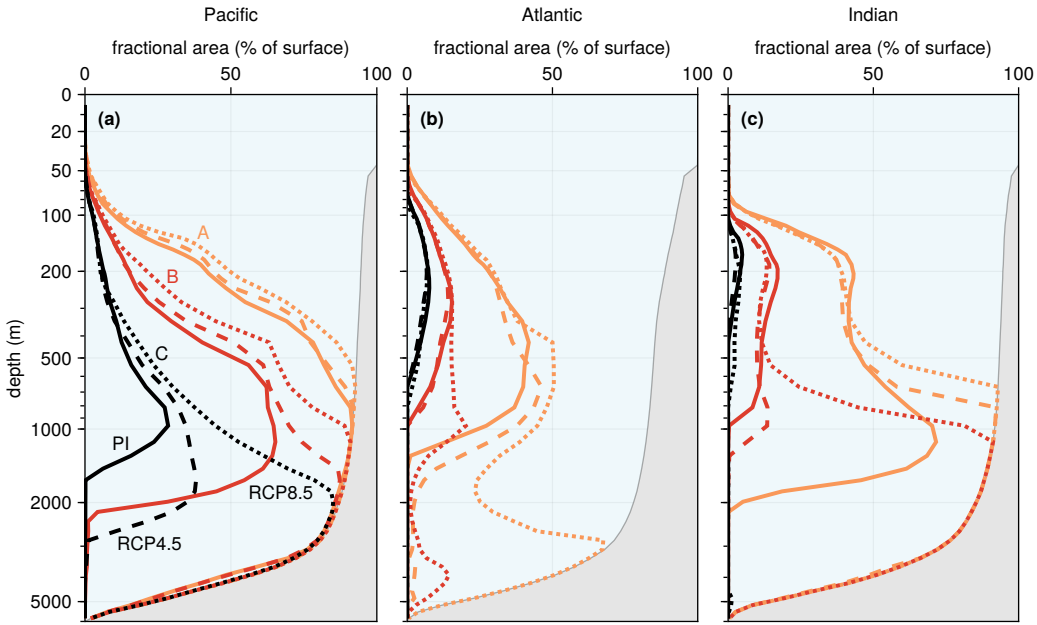


Figure 2. (a) Pacific depth profiles of the spatial extent of mild (A, orange; $pO_2 \leq 100$ matm), intermediate (B, red; $pO_2 \leq 50$ matm), and severe hypoxia (C, black; $pO_2 \leq 15$ matm) for the preindustrial state (PI; solid lines), the future RCP4.5-based state (dashed lines), and the future RCP8.5-based state (dotted lines). The spatial extent for a given hypoxia category and depth is quantified by the ratio of the horizontal hypoxic area to the surface area of the corresponding ocean basin. (The gray area represents the seafloor.) (b) As (a) for the Atlantic. (c) As (a) for the Indian Ocean. Note the nonlinear depth scale.

328 tion 2.6), over each basin, and for each scenario. The expansion of hypoxic regions is larger
 329 for RCP8.5 than for the less extreme RCP4.5 scenario. We find that low-oxygen condi-
 330 tions generally expand toward the seafloor in the deep ocean rather than toward the sur-
 331 face. In the Pacific, expansion is maximal with all abyssal waters becoming moderately
 332 hypoxic (cat. B; $pO_2 \leq 50$ matm) for RCP4.5 and severely hypoxic (cat. C; $pO_2 \leq 15$ matm)
 333 for RCP8.5. Similarly, all Indian Ocean waters below roughly 800 m become mildly hy-
 334 poxic for RCP4.5 and moderately hypoxic for RCP8.5. In the Atlantic, the volume of
 335 severe hypoxia changes little, while mild and intermediate hypoxia only strongly expand
 336 for RCP8.5 at intermediate and abyssal depths. In the Atlantic and Indian Ocean above
 337 500 m, the areal extent of hypoxia actually contracts slightly as pO_2 has slight increases
 338 there (cf., Fig. 1j-o discussed above).

To visualize the horizontal distribution of expanding hypoxic conditions, we consider the vertical water-column minimum pO_2 shown in Fig. 3. In the preindustrial state, oxygen minimum zones are located in the eastern tropical sectors of the major basins and in the North Pacific. In the future, global-scale expansion of low-oxygen conditions is visible for the RCP4.5-based state, except in the North Atlantic and in the Atlantic sector of the Southern Ocean, which remain ventilated ($pO_2 \geq 100$ matm) by NADW and an unrealistically deep Southern-Ocean mixed layer. Intermediate hypoxia expands southward beyond southern mid-latitudes, while severe hypoxia expands into the tropics. For the RCP8.5-based state, mild hypoxia occurs across the entire global ocean (although predominantly at depth as shown in Fig. 2), while intermediate hypoxia occurs across the entire Pacific, South Atlantic, and Indian Ocean, and severe hypoxia extends across the entire Pacific only, reaching as far as the Southern Ocean.

3.2 Drivers of deoxygenation

3.2.1 Changes in TOU and preformed oxygen

Deoxygenation occurs through declines in preformed oxygen and through increases in true oxygen utilization (TOU; see Methods, Section 2), which may also be thought of as negative regenerated oxygen (i.e., $O_2^{\text{reg}} = -\text{TOU}$; see, e.g., DeVries & Deutsch, 2014). Qualitatively, reduced respiration drives TOU decreases while a slower circulation drives TOU increases by allowing more time for respiration to act. Thus, TOU can either increase or decrease depending on which effect dominates (Appendix Fig. C1). We find that in the upper ocean TOU decreases because of reduced OUR and in the deep ocean TOU increases because of longer circulation timescales (upstream exposure times; Appendix Fig. C2). Preformed oxygen, by contrast, declines over most of the ocean (Appendix Fig. C1), in part because of warming-driven solubility decreases and importantly, as we will show below, because of an equatorward shift in ventilation. With warmer future sea surface temperatures (SSTs), surface O_2 concentrations decrease almost everywhere, except in the North Atlantic “cold blob” (e.g., Cheng et al., 2022) where temperatures decrease, and near the Weddell and Ross Seas where the mixed layer shoals (Appendix Fig. C3). Shoaling of the ACCESS model’s preindustrially deep mixed layer in these regions (see Fig. C2 in Pasquier, Holzer, Chamberlain, Matear, et al., 2023) considerably increases surface residence times, allowing preindustrially undersaturated O_2 to become more saturated despite the decreased solubility.

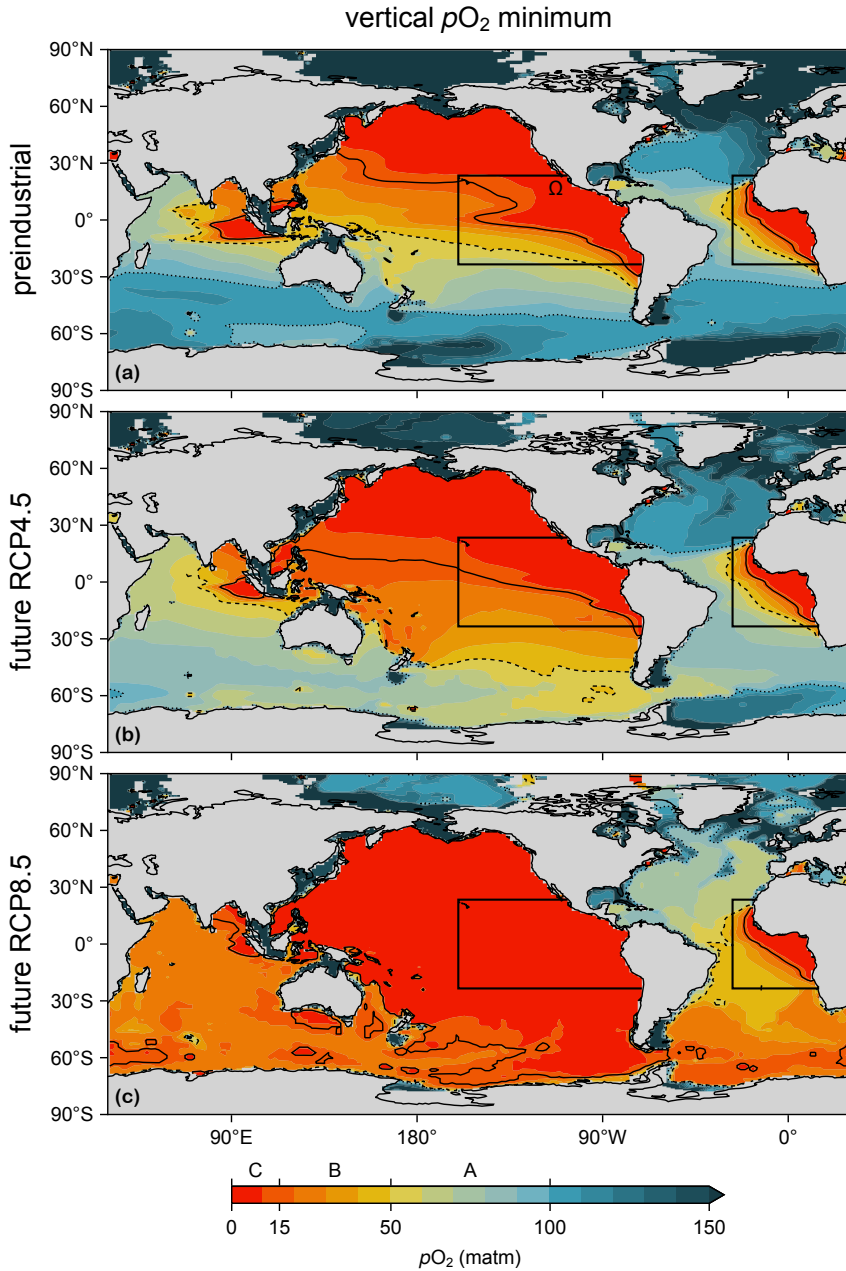


Figure 3. (a–c) Maps of the water-column minimum $p\text{O}_2$ for (a) the preindustrial state, (b) the future RCP4.5-based state, and (c) the future RCP8.5-based state. The dotted, dashed, and solid contour lines indicate the $p\text{O}_2 = 100$, 50, and 15 matm thresholds of hypoxia categories A, B, and C, respectively. Also indicated are the eastern tropical Pacific and Atlantic Ω regions over which our diagnostics are applied.

To analyze the drivers of deoxygenation in detail, we focus for definiteness on the eastern tropical Pacific (ETP, 23°S–23°N, east of 160°W) and eastern tropical Atlantic (ETA, 23°S–23°N, east of 27°W), as indicated in Fig. 3. Figure 4 shows the average O_2 depth profiles in these regions and their decomposition into O_2^{pre} and TOU. In the preindustrial state, both the ETP and ETA are severely hypoxic in the depth range of 150–800 m and 150–400 m, respectively. In the steady-state future scenarios, we find small upper-ocean O_2 decreases of about 10 μM above 70 m, caused by a decrease in O_2^{pre} . Decreases in O_2^{pre} are approximately constant with depth below ~ 100 m, while ΔTOU changes sign at ~ 1500 m in the ETP and at ~ 800 m in the ETA. Above ~ 500 m, the TOU decreases compensate almost perfectly for the O_2^{pre} decreases. Conversely, below ~ 2000 m, TOU increases and O_2^{pre} decreases compound, resulting in strong deoxygenation, with deep ETP O_2 reduced to $\sim 25\%$ of its preindustrial levels for RCP4.5 and to a mere $\sim 5\%$ for RCP8.5. Deep ETA O_2 decreases are of similar magnitude, but the preindustrial and future O_2 levels are roughly 100 μM higher owing to North Atlantic ventilation.

We now partition the changes ΔTOU and ΔO_2^{pre} into contributions from the key drivers, that is, into contributions from changes in circulation, respiration, and solubility (Methods, Section 2.5). For this purpose, we narrow our focus to the ETP only — similar mechanisms are at play in the ETA, but will not be discussed here for brevity. Guided by the shape of their profiles in Fig. 4, we furthermore integrate over the upper ETP (above 500 m) and separately over the deep ETP (below 2000 m) to summarize how different drivers dominate at different depths. The resulting attribution of ΔTOU and ΔO_2^{pre} to their drivers is shown in Fig. 5; we first discuss ΔTOU and then ΔO_2^{pre} .

3.2.2 Upper and deep ETP budgets of ΔTOU

The average TOU over a given region Ω is given by the global volume integral of the product of OUR with the upstream exposure time, Γ_Ω^\uparrow in steady state (see Methods, Section 2, Eq. (2); Holzer, 2022). This allows us to decompose ΔTOU into contributions from changes in respiration, from changes in circulation, and from their spatial correlations, which we refer to as the “cross term” in Eq. (3). These contributions are shown as the first three colored bars in each panel of Fig. 5.

In general terms, Figure 5 shows that the global decline in respiration acts toward decreasing TOU (green bars; note that Fig. 5 shows $\Delta O_2^{\text{reg}} = -\Delta\text{TOU}$), and hence in-

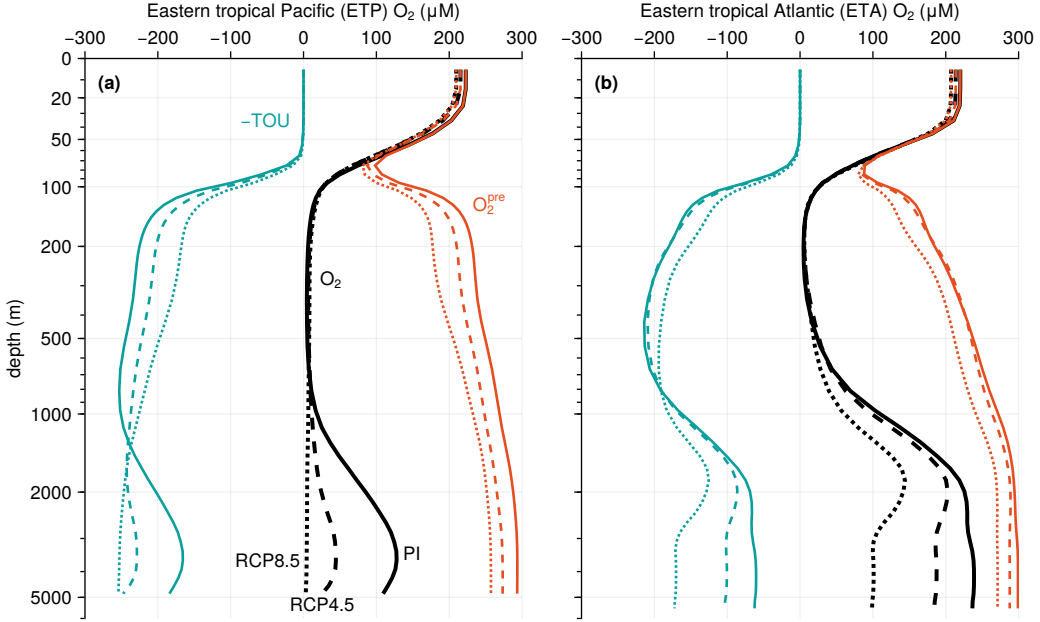


Figure 4. (a) Eastern tropical Pacific profiles of oxygen (O_2 , black), preformed oxygen (O_2^{pre} , orange), and true oxygen utilization (TOU, teal) for the preindustrial state (PI; solid line), the future RCP4.5-based state (dashed line), and the future RCP8.5-based state (dotted line). We show regenerated oxygen, $-TOU$, to show the effect of utilization on O_2 as additive. Note the nonlinear depth scale. (b) As (a) for the eastern tropical Atlantic. (The eastern tropical Pacific and Atlantic regions are defined in Fig. 3.)

402 increasing O_2 everywhere, as expected. Conversely, the slower future circulation increases
 403 TOU (blue bars) by increasing the upstream exposure time, allowing respiration, albeit
 404 at a reduced rate, to act over longer times. The magnitude of the cross-term contribu-
 405 tions to ΔTOU (orange bars) are generally on the same order as the circulation-only and
 406 respiration-only contributions, partly because of the large preindustrial-to-future changes
 407 considered here. Note that the ΔTOU cross term acts toward increasing O_2 because ΔOUR
 408 and $\Delta \Gamma_\Omega^\uparrow$ have opposite signs (negative contribution to ΔTOU). We now examine the
 409 drivers of TOU changes in detail for the upper and deep ETP.

410 For the upper ETP (Fig. 5a,c), respiration-driven TOU reduction (green bar) is closely
 411 compensated by circulation-driven TOU increases (blue bar). This shows that in the up-
 412 per ocean respiration is slower (driving TOU reductions of 23% and 36% for RCP4.5
 413 and RCP8.5), but the slower circulation allows this respiration to act for longer (driv-

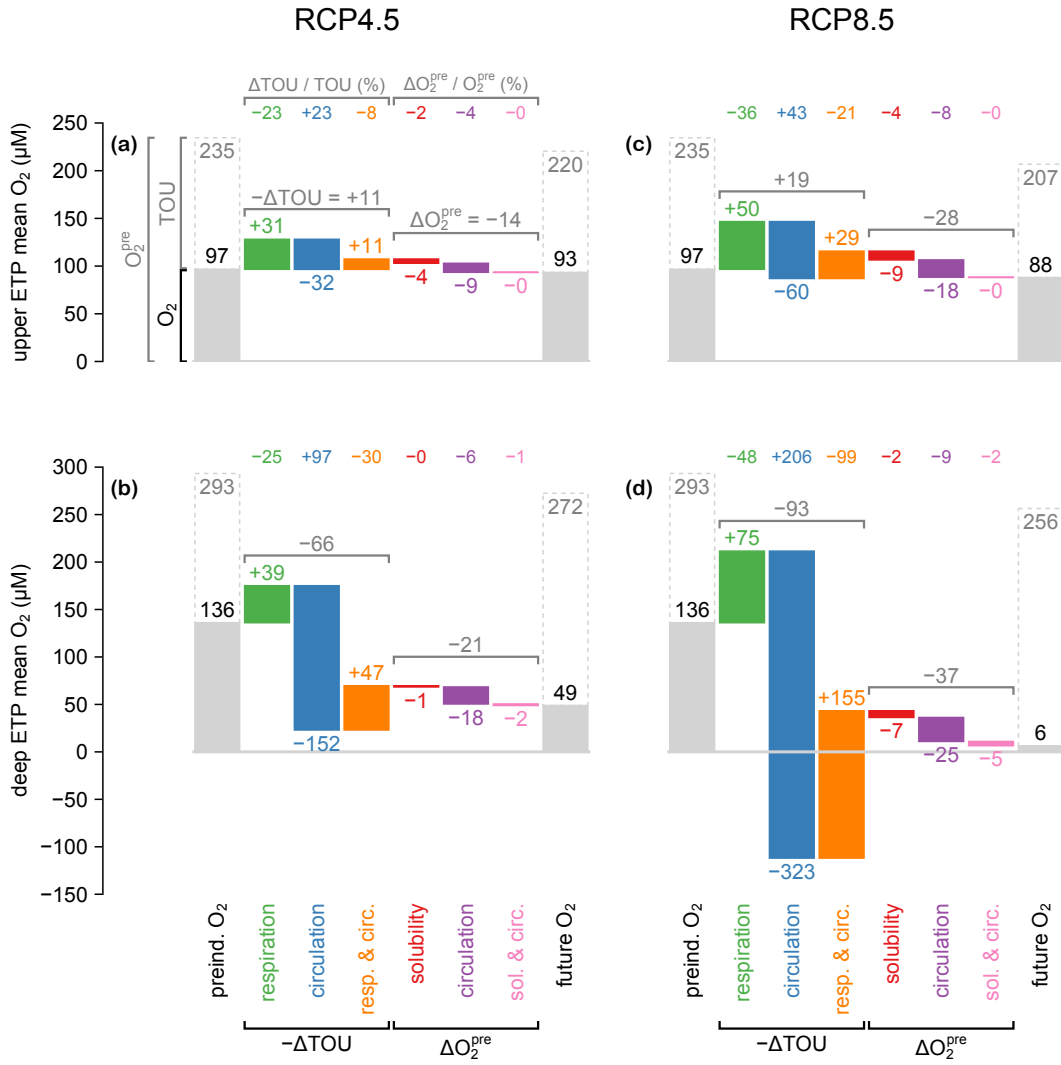


Figure 5. (a) ΔO_2 contributions for the upper ETP (0–500 m) for RCP4.5 plotted as a waterfall chart with the change from preindustrial O_2 (leftmost gray bar) to future O_2 (rightmost gray bar) decomposed into contributions (colored bars) that start where the previous one ends. ΔTOU is decomposed according to Eq. (3) into contributions from changes in respiration (green), circulation (blue), and their spatial covariance (orange). ΔO_2^{pre} is decomposed into contributions from solubility (red), circulation (purple), and their spatial covariance (pink). Percentage contributions to changes in TOU and O_2^{pre} are indicated at the top. (b) As (a) for the deep ETP (below 2000 m). (c–d) As (a–b) for RCP8.5.

ing TOU increases of 23 % and 43 %). As the effects of respiration-only changes (green bars) and circulation-only changes (blue bars) nearly cancel, the overall TOU decrease is driven by the spatial correlation between respiration changes and circulation changes

(orange bars). The concurrent increase of the circulation-only driven TOU and decrease of the respiration-only driven TOU must result in a negative cross term and hence in a TOU reduction, the precise magnitude of which depends on details of the underlying spatial patterns. The magnitude of the overall TOU decrease is about 8 % for RCP4.5 and 21 % for RCP8.5.

For the deep ETP, the circulation-only-driven Δ TOU (blue bars) dominates the other drivers with a magnitude that is roughly 5 times larger than for the upper ETP. In comparison, the magnitude of the respiration-only-driven Δ TOU (green bars) is only 30 % and 50 % larger for RCP4.5 and RCP8.5 than in the upper ETP. The respiration-driven decreases and circulation-driven increases in TOU again point to slower respiration acting for longer time. To quantify this, we calculated the upstream-exposure-time-weighted change in OUR and the OUR-weighted change in upstream exposure time to find that respiration slows by 25 % for RCP4.5 and 50 % for RCP8.5 but acts 2 times longer for RCP4.5 and 3 times longer for RCP8.5. For the deep ETP the cross terms (orange bars) are of the same order of magnitude as the respiration-only contribution (green bars), but the cross terms no longer dominate the overall TOU change as in the upper ETP. With all terms combined, the TOU of the deep ETP increases by 42 % for RCP4.5 and by 59 % for RCP8.5. A striking feature of these results is that, were respiration to be held constant at its preindustrial level, the Δ TOU contribution from the circulation slowdown alone (blue bars) is so strong that it would have the potential to remove the entire O_2 content of the deep ETP (filled gray bars) in the RCP4.5 scenario, and to do so more than two times over in the RCP8.5 scenario.

3.2.3 Upper and deep ETP budgets of ΔO_2^{pre}

The preformed oxygen content of volume Ω is controlled by euphotic O_2 concentrations and by the amount of the Ω volume that is ventilated per unit area at the base of the euphotic layer, $\mathcal{V}_\Omega^\downarrow$ (see Methods, Section 2, Eq. (4)). While $\mathcal{V}_\Omega^\downarrow$ depends only on the circulation, euphotic O_2 concentration is determined by both solubility and circulation through the subtle balance between air-sea gas exchange and euphotic-zone residence time. However, decomposing euphotic O_2 into saturation and disequilibrium components, O_2^{sat} and O_2^{dis} , allows us to separate solubility from circulation effects (including their spatial correlation “cross term” in Eq. (5)) because euphotic O_2^{sat} is determined by in situ solubility only, while euphotic O_2^{dis} is predominantly determined by circula-

449 tion. These contributions, volume integrated over either the upper or deep ETP, are also
 450 plotted as colored bars in Fig. 5.

451 Reduced surface solubility reduces the preformed oxygen inventory of the ETP by
 452 just a few percent (red bars) even for the extreme RCP8.5 case, accounting for less than
 453 $\sim 30\%$ of the overall O_2^{pre} decrease in the upper and deep ETP. The bulk ($\sim 70\%$ or more)
 454 of the overall order-10% decline in preformed oxygen is instead driven by changes in cir-
 455 culation (purple bars). The cross terms (pink bars) between already relatively small solubility-
 456 only and circulation-only contributions are essentially negligible. The circulation-only
 457 driven reductions in O_2^{pre} due to $\Delta V_\Omega^\downarrow$ represent re-arrangements in euphotic origin be-
 458 cause the area integral of V_Ω^\downarrow , which equals the volume of Ω , is constant across all states.
 459 The future decreases in the circulation-only contributions to ΔO_2^{pre} (computed with the
 460 preindustrial surface oxygen concentration) thus indicate a shift in ventilation pattern
 461 toward surface locations with lower oxygen concentration, i.e., toward warmer latitudes
 462 with lower solubility (see also Appendix Fig. C4). This equatorward shift in ventilation
 463 reduces the efficiency of the oxygen solubility pump and is the dominant driver of the
 464 decline in the preformed O_2 in both the upper and deep ETP.

465 It is interesting to note that regions with weaker future ventilation will have longer
 466 surface residence time and thus higher surface saturation, which can compensate for re-
 467 duced future solubility. In our model this occurs near the Weddell and Ross seas where
 468 the unrealistically deep preindustrial mixed layer shoals dramatically thereby increas-
 469 ing surface residence and saturation, which overwhelm the effect of reduced solubility
 470 leading to increased surface oxygen concentrations.

471 ***3.2.4 TOU changes in the ETP: three-dimensional distribution of TOU 472 origin***

473 Having quantified the globally integrated drivers of ETP deoxygenation, we now
 474 investigate their spatial distribution, beginning with the local contributions to TOU. The
 475 local contribution at point \mathbf{r} to the TOU inventory of region Ω is given by the product
 476 $\Gamma_\Omega^\uparrow(\mathbf{r}) \text{OUR}(\mathbf{r})$, which quantifies the origin of the TOU inventory, i.e., the oxygen loss
 477 that occurred at \mathbf{r} upstream of Ω . Figures 6 and 7 show the TOU origin for the upper
 478 and deep ETP, respectively. The zonally integrated TOU origin is plotted for the prein-
 479 dustrial state together with its futures changes.

480 For the upper ETP (Fig. 6), TOU originates almost exclusively in the Pacific, pre-
 481 dominantly in thermocline waters across all non-polar latitudes, with peak contributions
 482 at a depth of \sim 200 m. Thus, there is significant oxygen loss within the upper-ocean cir-
 483 culation as it transports oxygen to the upper ETP. TOU in the upper ETP also orig-
 484 inates at depths between 1000–2000 m at low and high latitudes, where upwelling old oxy-
 485 gen is intercepted by the bacterial respiration of abundant sinking organic matter be-
 486 neath high productivity. For both RCP4.5 and RCP8.5, the change in TOU origin re-
 487 veals a shoaling (upward shift) of the average location where oxygen bound for the up-
 488 per ETP is lost. This shift presumably occurs because the slower future circulation al-
 489 lows respiration to act for longer so that oxygen bound for the upper ETP is stripped
 490 out higher in the water column. The TOU origin below the thermocline at low and high
 491 latitudes decreases, presumably because of reduced biological productivity and subja-
 492 cent respiration, as well as a lower O_2 content of the water that upwells there. The up-
 493 ward shift in TOU origin and reduced deep origin are thus both consequences of respi-
 494 ration removing oxygen sooner, i.e., further upstream, during its transit from the euphotic
 495 zone.

496 For the deep ETP (Fig. 7), TOU originates in every ocean basin. The Atlantic makes
 497 a 20 % contribution and the Indian Ocean a 15 % contribution, mostly at high latitudes
 498 known to ventilate the deep Pacific (e.g., Holzer et al., 2021). For all basins, the largest
 499 TOU origin lies in upper thermocline waters where most respiration occurs. Deeper TOU
 500 origin at high latitudes, and in the Pacific throughout the water column at low latitudes,
 501 occurs below regions of vigorous biological production where respiration is high. The fact
 502 that the low-latitude tongue of oxygen loss in the Pacific lies partly above, and hence
 503 *down-stream* of the deep ETP, implies that either some O_2 is utilized as it mixes diffu-
 504 sively downward, or, more likely, that water destined to be carried by meridional over-
 505 turning back to the deep ETP at depth has its oxygen stripped out in the upwelling branch
 506 of the overturning. Consistent with such an overturning pathway, local maxima of TOU
 507 origin occur in the mid-depth North Pacific and in the abyssal Pacific sector of the South-
 508 ern Ocean.

509 The changes in the TOU origin of the deep ETP plotted in Fig. 7 show a global in-
 510 crease and upstream intensification of the removal of oxygen destined for the deep ETP.
 511 For the RCP4.5-based future state, the TOU origin increases mostly near the surface of
 512 the Pacific, South Atlantic, and southern Indian Ocean where it was already large in the

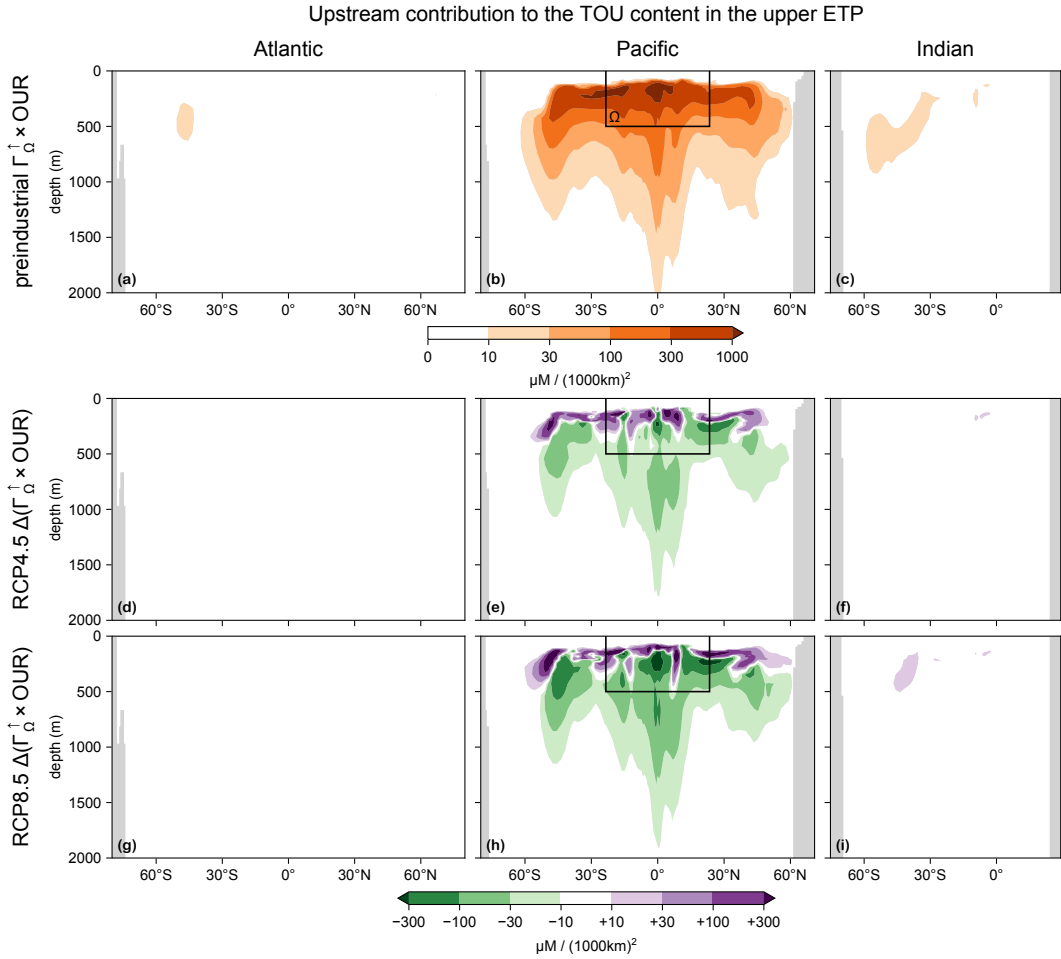


Figure 6. Upstream contribution to the TOU in the upper ETP (0–500 m; indicated by the solid black line; subvolume Ω in our equations) as quantified by basin zonal integrals of $\Gamma_{\Omega}^{\uparrow} \times \text{OUR}$ normalized by the ETP volume for the Atlantic (a), Pacific (b), and Indian Ocean (c). (d–f) As (a–c) for the future change in the RCP4.5-based scenario. (g–i) As (d–f) for RCP8.5. Note the nonlinear color scale and that the normalized zonal integrals plotted give the contribution per unit latitude–depth area.

513 preindustrial state. For RCP8.5, the TOU contributions are generally stronger and, un-
 514 like for RCP4.5, they also increase near the North Atlantic surface. However, in the old
 515 waters of the mid-depth North Pacific the TOU origin of the deep ETP actually decreases
 516 for RCP8.5, likely because of shifts in production, and hence respiration, away from the
 517 surface origin of these old waters so that less oxygen is stripped out of them in the fu-
 518 ture.

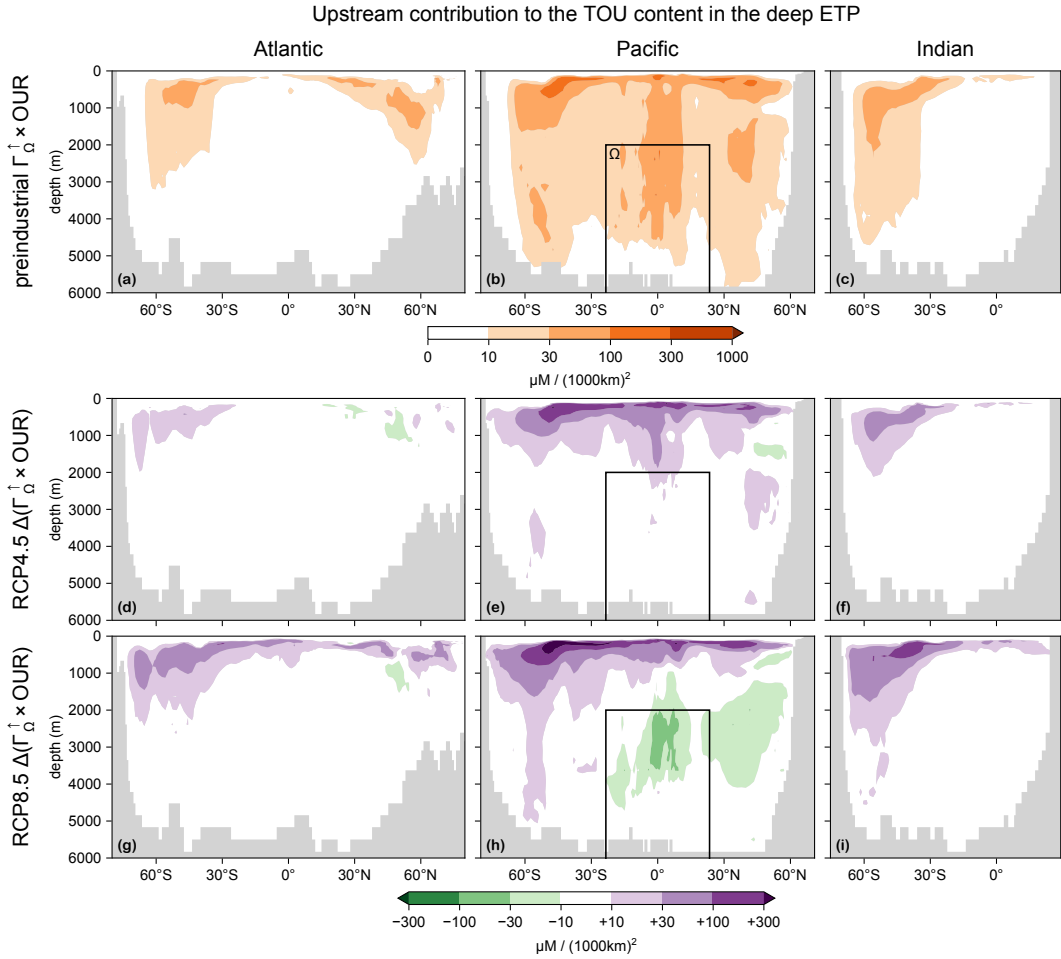


Figure 7. As Fig. 6 for the deep ETP (below 2000 m; indicated by the solid black line).

519 **3.2.5 Preformed oxygen changes in the ETP: shifting ventilation patterns**

520

521 Here we take a closer look at the geographic shifts in ventilation patterns that drive
 522 the decreased preformed oxygen content of the ETP. The amount of O_2^{pre} supplied to Ω
 523 from euphotic location r is quantified by the product $O_2(r) \mathcal{V}_\Omega^\downarrow(r)$, maps and zonal in-
 524 tegrals of which are plotted in Fig. 8 for the preindustrial state and the future changes.
 525 (Corresponding plots of $\mathcal{V}_\Omega^\downarrow$ by itself, shown in Appendix Fig. C4, share strong simila-
 526 rities with Fig. 8, underscoring that changes in ventilation patterns are the dominant driver
 527 of ΔO_2^{pre} .)

528 For the upper ETP, the origin of preformed oxygen in the preindustrial state (Fig. 8a)
 529 shows that while much oxygen comes from the overlying surface, a considerable fraction

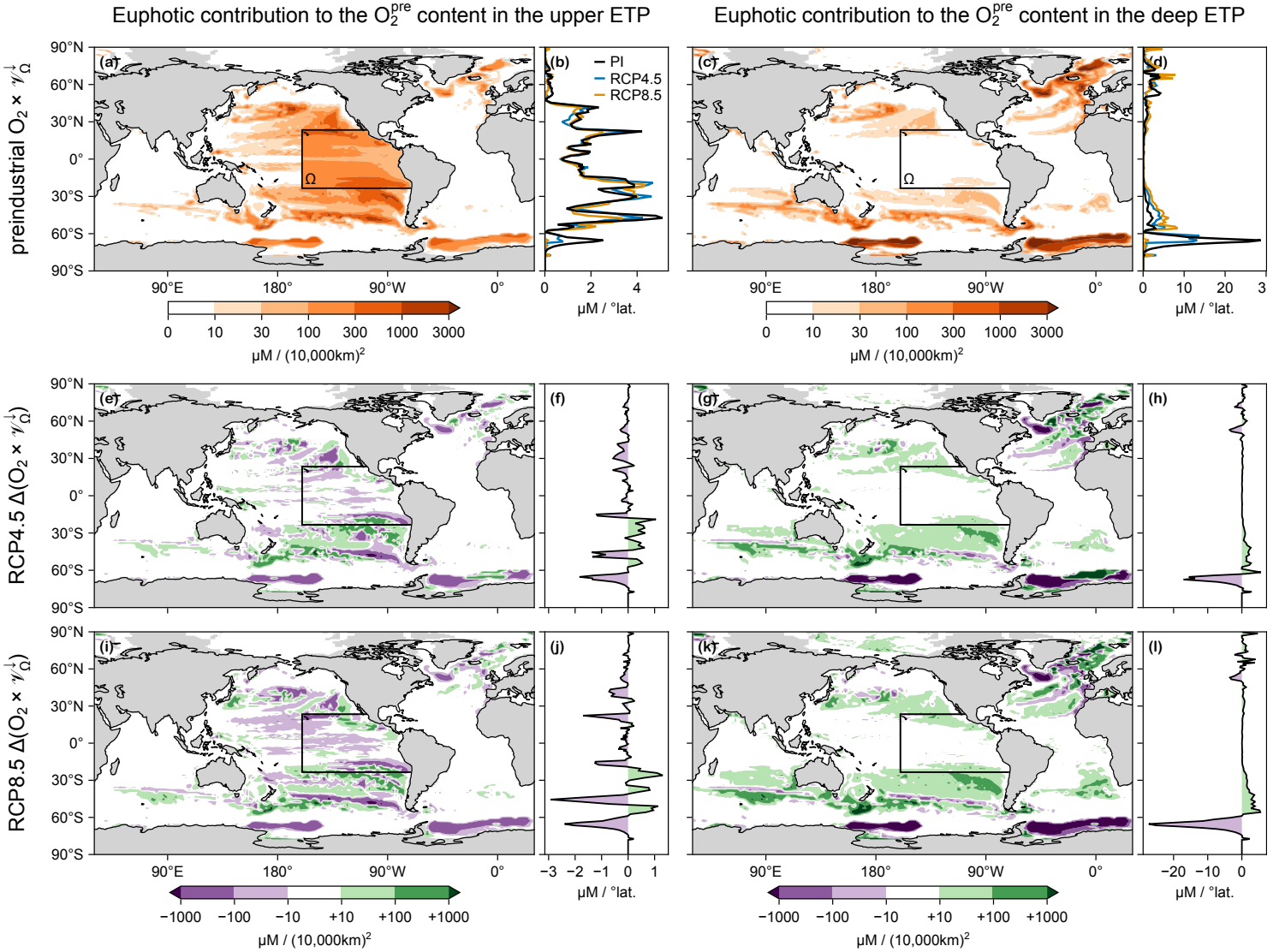


Figure 8. (a) Map and (b) zonal integral of the euphotic contribution to the mean O_2^{pre} in the upper ETP (subvolume Ω indicated by a solid black contour), as quantified by $O_2 \times \mathcal{V}_\Omega^\downarrow$ normalized by the volume of Ω , in the preindustrial state. (c–d) As (a–b) for Ω the deep ETP. (e–h) As (a–d) for $\Delta(O_2^{\text{pre}} \times \mathcal{V}_\Omega^\downarrow)$ for the RCP4.5 scenario. (i–l) As (e–h) for RCP8.5. Note the nonlinear color scale and that the contributions plotted are per unit horizontal area.

530 is supplied from Mode and Intermediate water-formation regions in the Pacific, and from
 531 deep-water formation regions in the Southern Ocean (Weddell and Ross Seas) and North
 532 Atlantic. For deep ETP in the preindustrial state, the tropical and subtropical contrib-
 533 utions are much weaker while contributions from the deep-water formation regions of
 534 the Southern Ocean and the North Atlantic are more important.

535 For the future changes, the largest decreases in preformed oxygen origin occur in
 536 the deep-water formation regions, particularly near the Weddell and Ross Seas. The sup-
 537 ply of O_2^{pre} from south of 60°S declines by about 70 % and 50 % for the upper and deep
 538 ETP, respectively, for the RCP4.5 scenario, and almost completely shuts down for both
 539 the upper and deep ETP for RCP8.5. As discussed for Fig. 5 and underscored by the sim-
 540 ilarity between Fig. 8 and Appendix Fig. C4, this is dominantly due to circulation-driven
 541 changes in ventilation. Large-scale increases of the O_2^{pre} supply are most prominent in
 542 the subtropical gyres, which become more important oxygen sources for the ETP in the
 543 future.

544 4 Discussion

545 We investigated the future deoxygenation of the ocean for idealized steady states
 546 of the oxygen cycle in equilibrium with the mean 2090s physical ocean state as predicted
 547 for the RCP4.5 and RCP8.5 scenarios. To attribute future changes to their drivers, we
 548 focused on the eastern tropical basins (primarily the Pacific) as these contain OMZs in
 549 the current ocean, and because their future deoxygenation is typical of the large-scale
 550 response in our model. The key driving mechanisms were quantified by decomposing the
 551 oxygen changes into contributions from changes in surface solubility, ocean circulation,
 552 and oxygen utilization rates. Here we discuss caveats of our approach and compare our
 553 results to previous work.

554 4.1 Caveats

555 A number of caveats must be kept in mind when interpreting our findings. Some
 556 caveats also apply to the nutrient and carbon cycles and have been previously discussed
 557 by Pasquier, Holzer, Chamberlain, Matear, et al. (2023) and Pasquier, Holzer, and Cham-
 558 berlain (2023). Below we detail the caveats that specifically apply to our analysis of de-
 559 oxygenation.

560 (i) The circulation models used here are steady, while the real ocean circulation is in a
561 transient state that is currently slowing down due to climate change (e.g., Srokosz & Bry-
562 den, 2015). Given the wide range of transit times in the ocean (e.g., Primeau, 2005), the
563 ocean circulation will keep changing well beyond the 21st century until eventually re-
564 turning to an approximate equilibrium after a few millennia (e.g., Schmittner et al., 2008),
565 which is a different state from those considered here. Oxygen distributions are thus not
566 expected to be anywhere near steady by the end of the 21st century (e.g., Shaffer et al.,
567 2009). Our biogeochemical states should not be interpreted as predictions of the future,
568 but they do capture key mechanisms that shape the real ocean's response to climate change
569 on long time scales. Furthermore, our steady-state framework does not account for sea-
570 sonal variations. We therefore cannot capture the effects from seasonally covarying fluc-
571 tuations of biology, physics, and thermodynamics, which play a significant role in the sea-
572 sonal oxygen fluctuations of the upper few hundred meters as seen in both observations
573 and models (see, e.g., Jin et al., 2007; Graco et al., 2017; Espinoza-Morriberón et al., 2021;
574 Pitcher et al., 2021, to cite a few).

575 (ii) Our results are specific to the circulation models used here to some extent. Apart
576 from the steady-state issues, flaws of the ocean circulation model, such as the unreal-
577 istically deep mixed layer of the preindustrial state inherited from the parent ACCESS1.3
578 model (Bi et al., 2013) and its shoaling in the future, leave a pronounced imprint on our
579 results. However, the mechanisms through which changes in circulation affect deoxygena-
580 tion should be model-independent. For example, a future Southern Ocean ventilation
581 decline (which is expected alongside shoaling mixed layers; see, e.g., de Lavergne et al.,
582 2014; Kwiatkowski et al., 2020) will reduce preformed O₂ by shifting its surface origin
583 toward warmer waters while a generally slower circulation will increase TOU by allow-
584 ing respiration to act over longer timescales.

585 (iii) Our results are also specific to the biogeochemistry model employed (PCO2; Pasquier,
586 Holzer, Chamberlain, Matear, et al., 2023), which was designed to be relatively simple
587 and does not explicitly represent every mechanism at play. Potentially important miss-
588 ing mechanisms include feedbacks from the nitrogen cycle, which are linked to oxygen
589 through denitrification and nitrification. Denitrification, which is only modelled implic-
590 itly in PCO2 (see Methods, Eq. (1)), is important because anaerobic respiration in low
591 oxygen environments acts as an effective oxygen source. Conversely, nitrogen fixation
592 and nitrification, which produce nitrite and nitrate by consuming oxygen, are not rep-

resented at all in PCO₂. Effects from the nitrification–denitrification imbalance on the oxygen cycle, expected to contribute about two thirds of a ~6 % increase in the global O₂ inventory by the year 8000 (Oschlies et al., 2019), are therefore not captured in our model. However, we note that this imbalance is expected to be dominated by denitrification (which *is* parameterized in PCO₂) and remains secondary for the first few centuries of sluggish circulation until about the year 5000 when the overturning circulation recovers.

600 4.2 Relation to previous work

Because our analysis is framed for steady state, we do not expect a detailed match with previous studies based on transient simulations. We do, however, expect similarities with simulations that last long enough for the effect from slow processes to manifest. In particular, this includes processes mediated by the deep ocean circulation, which is the dominant driver of deoxygenation in our analyses and operates on multi-centennial timescales (e.g., Primeau, 2005), with effects that will not have asserted themselves by the end of the 21st century (e.g., Moore et al., 2018). However, the relatively more sluggish ocean state predicted for the next few centuries will likely only be temporary. A more vigorous circulation is expected to return after several millennia as deep ocean temperatures equilibrate (e.g., Schmittner et al., 2008). We therefore expect our results to be generally closer to century-scale predictions than to predictions for thousands of years in the future. We also note that differences in biogeochemistry, in ocean circulation, in scenarios and forcings, and so on, further complicate quantitative comparisons.

In terms of deoxygenation, our results agree qualitatively with predictions for the end of the 21st century but differ in magnitude, particularly at depth. For the upper ocean, Kwiatkowski et al. (2020) reported a (10±2) % decline in 100–600 m deep oxygen across CMIP5 models and a (13±5) % decline across CMIP6 models for RCP8.5 and SSP5-8.5, respectively, compared to the ~20 % decline for our RCP8.5-based future steady state. (CMIP6 uses the “Shared Socioeconomic Pathway” (SSP) classification (Riahi et al., 2017) where SSP5-8.5 nominally matches RCP8.5 (Arias et al., 2021).) Similarly, for RCP4.5, Kwiatkowski et al. (2020) reported a 6±3 % decline for CMIP5 and a 8±4 % decline for CMIP6, compared to a ~7 % decline in this study for the same scenario. Near the sea floor, Kwiatkowski et al. (2020) reported a weak but consistent 6±2 % oxygen decline across CMIP6 models and scenarios, compared to a much stronger ~40 % and ~80 %

625 decline in the abyss of our RCP4.5- and RCP8.5-based states, respectively. The volumes
 626 of our future steady-state hypoxic regions thus are dramatically larger than the future
 627 predictions of a moderate ~10 % expansion in mild hypoxia and a contraction of the OMZ
 628 core (e.g., Gnanadesikan et al., 2012; Busecke et al., 2022). The large differences seen
 629 here mostly at depth are driven by circulation changes that act in perpetuity, but cor-
 630 responding effects in transient simulations have not fully developed by 2100.

631 Longer-term transient simulations in principle allow for closer comparisons with
 632 our steady states but the recovery of the ocean circulation intervenes before the effects
 633 of circulation slowdown on oxygen can fully develop. Running a climate model with $p\text{CO}_2$
 634 at three times its preindustrial level from 2100 onward, Matear and Hirst (2003) reported
 635 a ~30 % decline in O_2 below 4000 m by 2700. This O_2 decline is larger than those es-
 636 timated for 2100 but still far from the corresponding 80 % decline of our RCP8.5-based
 637 state, because the circulation effects on O_2 are not fully developed as evidenced by a deep
 638 O_2 trend that remains strongly negative by 2700. Matear and Hirst (2003) report spa-
 639 tial patterns that are similar to our steady-state responses, with intense O_2 declines in
 640 the deep Southern Ocean driven by decreased ventilation. However, the simulation by
 641 Matear and Hirst (2003) was not continued beyond 2700, which is roughly when the cir-
 642 culation is expected to start recovering. In a multimillennial double- $p\text{CO}_2$ simulation,
 643 Frölicher et al. (2020) find a 700-yr decline in O_2 mostly below 2000 m accumulating to
 644 a ~10 % loss globally (compared to 40 % for our RCP4.5-based state) before O_2 slowly
 645 increases again over multiple millennia driven by the recovery of Southern-Ocean ven-
 646 tilation. In another multimillennial simulation with $p\text{CO}_2$ reaching almost 2000 μatm around
 647 year 2300 and slowly declining to ~1200 μatm over the next five millennia, Oschlies et
 648 al. (2019) find an O_2 decline of ~25 %, also reached around year 2700, before O_2 levels
 649 increase again with the recovering circulation.

650 Our analyses differ from previous studies in attributing deoxygenation to specific
 651 mechanisms. In our work here, solubility alone accounts for less than 10 % of the global
 652 O_2 decline, which is lower than previous estimates. However, despite some consensus,
 653 previous studies likely overestimate the solubility contribution. Studies that infer the sol-
 654 ubility contribution from a residual, typically between a climate-change simulation and
 655 a similar simulation with the solubility fixed to preindustrial values (e.g., Matear & Hirst,
 656 2003), unintentionally include effects from changes in ventilation patterns (which should
 657 be attributed to circulation change) because the residual includes spatial correlation (“cross”)

658 terms, which we estimate to be order 20 %. Approximations based on heat flux gener-
659 ally overestimate the contribution from solubility changes because they assume complete
660 saturation (e.g., 20 %–30 %; Bopp et al., 2002; Palter & Trossman, 2018). Solubility-change
661 contributions quantified through an abiotic/preformed O₂ tracer are generally overes-
662 timated yet more (e.g., 30 %–50 %; Oschlies et al., 2019; Oschlies, 2021) because the pre-
663 formed tracers respond to both saturation and circulation changes. Similarly, solubil-
664 ity contributions quantified directly by the change in saturation concentration as a func-
665 tion of in situ temperature and salinity are overestimated even more (e.g., 40 %–70 %;
666 Frölicher et al., 2020). Only studies that perturb surface solubility alone, e.g., by pre-
667 scribing the future surface temperature for the solubility in an otherwise unperturbed
668 preindustrial state, can provide unbiased estimates. This includes, e.g., the 15 %, 25 %,
669 and 35 % estimates by Matear et al. (2000), Bopp et al. (2002), and Plattner et al. (2001),
670 respectively (the differences likely stemming from model-specific biases, with higher es-
671 timates corresponding to states with smaller changes in Southern-Ocean ventilation.) Given
672 these overestimates of solubility-change contributions to the ocean oxygen inventory, and
673 given that spatial correlations between changes in ventilation patterns and solubility are
674 typically overlooked, it is likely that previous studies have typically underestimated the
675 effects from circulation changes.

676 5 Conclusions

677 We quantified the drivers of large-scale ocean deoxygenation in future steady states
678 corresponding to perpetual 2090s conditions. This was done by embedding the PCO₂
679 model into the average ocean state as predicted for the 2090s by the ACCESS climate
680 model for the RCP4.5 and RCP8.5 scenarios and solving directly for the biogeochem-
681 ical steady state. Future changes were evaluated relative to a steady preindustrial state
682 and analyzed for the eastern tropical Pacific (ETP), which contains the largest hypoxic
683 volume. We partitioned changes in TOU and preformed oxygen into their drivers, i.e.,
684 into contributions from changes in circulation, respiration, solubility, and their interac-
685 tions (cross terms).

686 Key to our being able to isolate — for the first time — the role of circulation changes
687 in driving deoxygenation is the conceptually novel upstream exposure time, a circula-
688 tion timescale that controls the oxygen content of a given subvolume Ω of the ocean. Specif-
689 ically, it is the time for which the oxygen that is “missing” from Ω was exposed to up-

stream respiration. The upstream exposure time thus provides the precise connection between TOU and OUR (Holzer, 2022) and, as shown here, the precise link between ventilation volume and preformed oxygen. In essence, the upstream exposure time, which is determined by the circulation only, traces TOU and preformed oxygen back in time to their origin.

Our main conclusions are as follows:

1. Keeping the ocean in a perpetual 2090s state leads to steady-state oxygen distributions characterized by intense global-scale deoxygenation at depth. Global oxygen inventories decline by 30 % and 60 % for the RCP4.5- and RCP8.5-based states, respectively. For the extreme RCP8.5 case, Pacific abyssal waters become severely hypoxic ($pO_2 \leq 15 \mu\text{M}$) over the entire basin, while Atlantic and Indian Ocean abyssal waters become mildly hypoxic ($pO_2 \leq 100 \mu\text{M}$) everywhere. The extent of hypoxic regions in the upper ocean changes remarkably little in our idealized future states, owing to decreased preformed oxygen being compensated by reduced TOU.
2. Intense deep-ocean TOU increases are dominantly driven by the slower future circulation allowing respiration to act over longer times while modest upper-ocean TOU decreases are characterized by close compensation between respiration-only and circulation-only effects. Specifically, in the deep ETP, TOU increases by 50 % and 100 % for RCP4.5 and RCP8.5 driven by 2–3 times longer upstream exposure to respiration, which overwhelms the decline in respiration rates, while in the upper ETP, TOU decreases by about 10 %. Thus, despite the global decline in respiration rates, the circulation slowdown drives intense deoxygenation at depth and prevents increased oxygenation in the upper ocean.
3. Preformed oxygen declines virtually everywhere driven mostly by shifts in ventilation patterns, rather than by the decrease in solubility due to warmer future sea surface temperatures. More than 70 % of the decline in preformed oxygen is driven by the origin of preformed oxygen shifting away from high latitudes toward lower latitudes, where warmer waters hold less oxygen. In situ warming-driven solubility reductions by themselves, at fixed circulation, reduce preformed oxygen by only ~30 % in the upper ETP and by less than 20 % in the lower ETP, accounting for less than 10 % of the overall deoxygenation. Thus, while preformed oxy-

722 gen is often thought to decrease because of warming-driven reduced solubility (e.g.,
723 Palter & Trossman, 2018; Oschlies et al., 2019; Couespel et al., 2019; Oschlies, 2021),
724 our analysis reveals that instead the change in ventilation pathways is the dom-
725 inant driver.

726 Our work demonstrates that if the oxygen cycle were allowed to come to equilibrium with
727 a permanently slower future ocean circulation, it would be the circulation changes that
728 are the dominant driver of both declines in preformed oxygen and increases in TOU. To
729 understand the fate of oxygen in the future ocean, it is therefore important to carefully
730 quantify ventilation patterns and key ocean circulation timescales, such as the upstream
731 exposure time, in simulations of the future ocean. The necessary computations can ef-
732 ficiently be performed by building the associated transport matrices as was done here
733 and which we hope will become a more widely adopted practice.

734 **Appendix A Model–observations comparisons**

735 Figure A1 shows the basin zonal-mean pO_2 for the preindustrial state of our model
 736 and for the GLODAPv2 observations, along with the corresponding mismatch. The un-
 737 realistically deep mixed layers of the Southern Ocean in the parent model manifest as
 738 overestimated pO_2 in the Atlantic and Pacific south of 60°S. Other systematic model bi-
 739 ases are visible, for example in the northern Indian Ocean, where PCO2 overestimates
 740 pO_2 , and in the tropical and subtropical upper Atlantic and Pacific, where PCO2 un-
 741 derestimates pO_2 .

742 Figure A2 shows the areal extent of each hypoxia category in each ocean basin as
 743 modelled for the preindustrial state and as captured by the GLODAPv2 observations.
 744 The extent of the Atlantic and Pacific hypoxic areas is generally overestimated, while
 745 the extent of the Indian-Ocean hypoxic areas is generally underestimated particularly
 746 at depth, consistent with Fig. A1. We note that the pO_2 thresholds used are different
 747 for model and observations as they were adjusted for the model so that the global hy-
 748 poxic volume for a given category is the same for the model as for GLODAPv2 (Meth-
 749 ods, Section 2.6). (Note that the global match does not guarantee matching volumes within
 750 a given basin.)

751 Figure A3 shows the geographic distribution of hypoxic waters as quantified by the
 752 water-column minimum of pO_2 for the preindustrial model state and for the GLODAPv2
 753 observations. While the large-scale patterns seen in the observations are captured by the
 754 model, there are significant mismatches. The underestimated pO_2 in the Pacific and At-
 755 lantic manifest as OMZs (hypoxia category C) that are larger than observed. The model
 756 places the Indian Ocean OMZ southeast of western Indonesia while observations show
 757 it to occur in the Bay of Bengal and in the Arabian Sea.

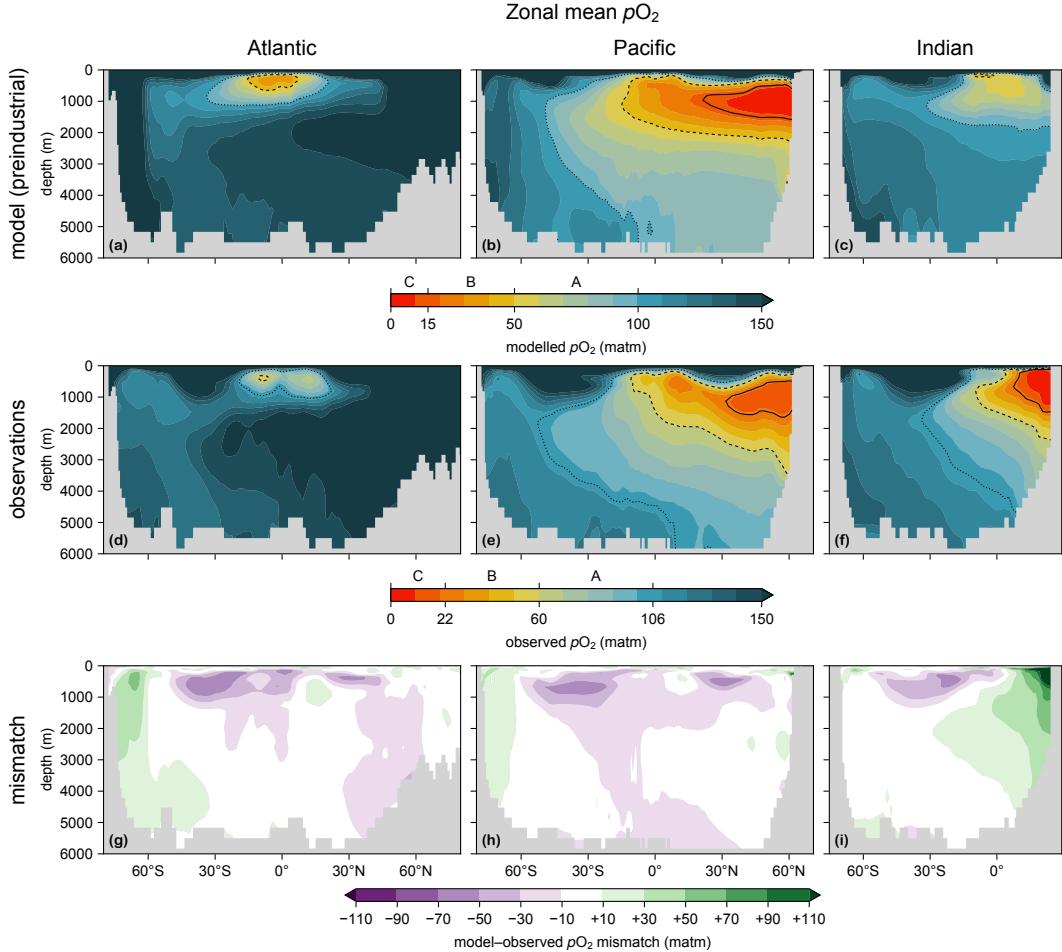


Figure A1. (a) Atlantic, (b) Pacific, and (c) Indian Ocean zonal mean $p\text{O}_2$ for the pre-industrial state. The dotted, dashed, and solid contour lines indicate the thresholds of hypoxia categories A, B, and C, respectively (which are different for model and observations; see Methods, Section 2.6). (d–f) As (a–c) for observations. (g–i) As (a–c) for the model–observations mismatch. The Atlantic basin excludes the Gulf of Mexico and the Caribbean, and the Pacific basin excludes the Sea of Japan so that the zonal means are more cleanly interpretable.

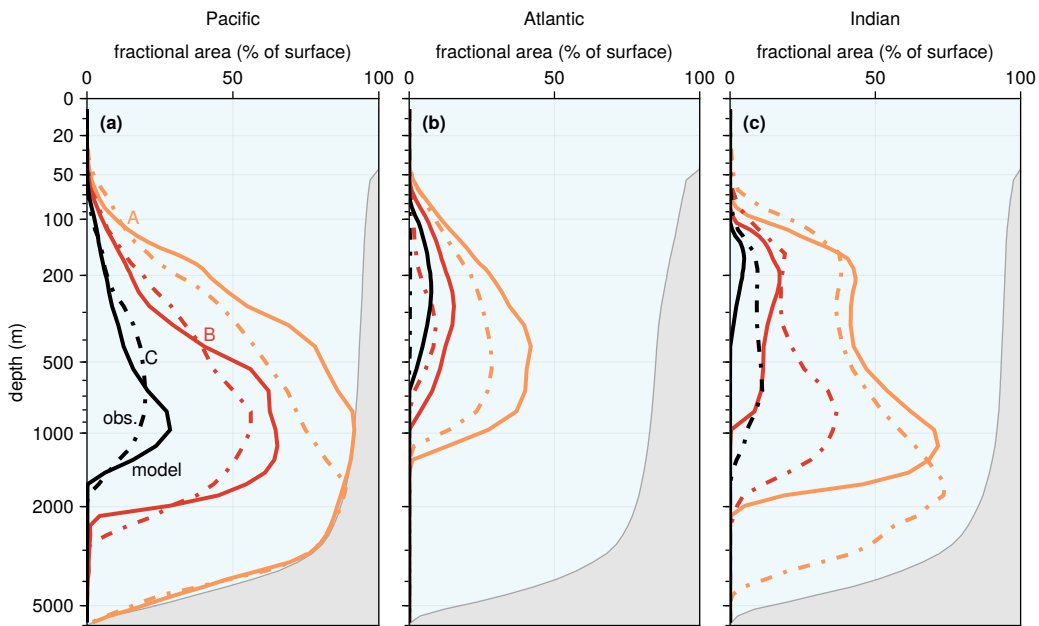


Figure A2. (a) Pacific depth profiles of the spatial extent of mild (A, orange), intermediate (B, red), and severe hypoxia (C, black) for the modelled preindustrial state (model; solid lines) and the observations (obs.; dash-dotted lines). (b) As (a) for the Atlantic. (c) As (a) for the Indian Ocean. (The gray shading represents the seafloor.) Note the nonlinear depth scale and that the $p\text{O}_2$ thresholds used for model and observations are different (see Methods, Section 2.6).

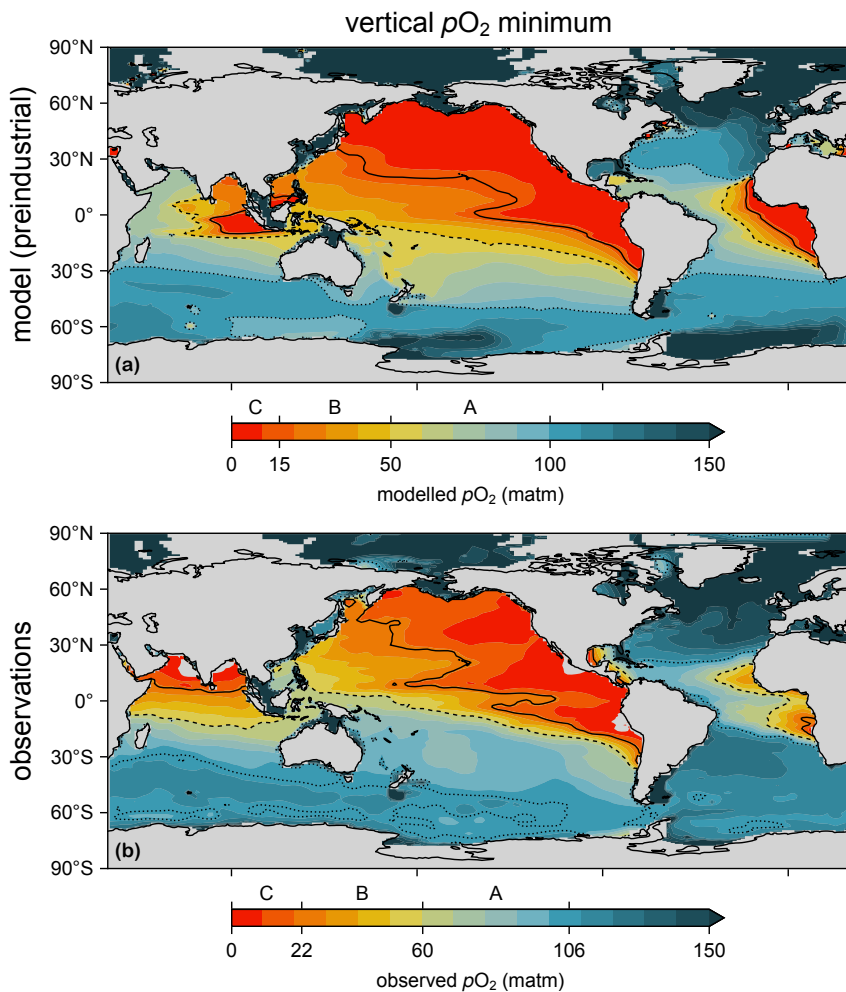


Figure A3. (a–b) Maps of the water-column minimum $p\text{O}_2$ for (a) the modelled preindustrial state and (b) observations. The dotted, dashed, and solid contour lines indicate the thresholds of hypoxia categories A, B, and C, respectively (which are different for model and observations; see Methods, Section 2.6).

758 Appendix B Mathematical and computational details

759 We organize the grid values of concentrations into column vectors and discretized
 760 linear operators into corresponding sparse matrices. In matrix form, the vector of pre-
 761 formed oxygen, $\mathbf{O}_2^{\text{pre}}$, is conveniently computed by solving $(\mathbf{T} + \mathbf{L}) \mathbf{O}_2^{\text{pre}} = \mathbf{L} \mathbf{O}_2$, where
 762 \mathbf{T} is the discretized advective-diffusive flux-divergence operator (“transport matrix” for
 763 short), and \mathbf{L} is a diagonal matrix with diagonal values of 1 s^{-1} in the euphotic zone and
 764 0 otherwise, enforcing $\mathbf{O}_2^{\text{pre}} = \mathbf{O}_2$ in the euphotic zone (only the euphotic-zone values of
 765 \mathbf{O}_2 are used in $\mathbf{L} \mathbf{O}_2$). (For such short (1 s) relaxation times there is no sensitivity to
 766 the precise value of that relaxation time; for example, using 10 s would give indistinguish-
 767 able results.) The vector of TOU grid values is similarly conveniently computed from
 768 OUR by solving $(\mathbf{T} + \mathbf{L}) \mathbf{TOU} = \mathbf{OUR}$ (Holzer, 2022).

769 In matrix form, Eq. (2) becomes $\boldsymbol{\Omega}^\top \mathbf{V} \mathbf{TOU} = \mathbf{OUR}^\top \mathbf{V} \boldsymbol{\Gamma}_\Omega^\uparrow$ where \mathbf{V} is a diag-
 770 onal matrix with the grid-box volumes along the diagonal, $\boldsymbol{\Omega}$ is a mask vector with en-
 771 tries of 1 for grid cells in Ω and entries of 0 otherwise, and the $^\top$ superscript denotes the
 772 matrix transpose. The upstream exposure time obeys $(\tilde{\mathbf{T}} + \mathbf{L}) \boldsymbol{\Gamma}_\Omega^\uparrow = \boldsymbol{\Omega}$ (Holzer, 2022),
 773 where $\tilde{\mathbf{T}} = \mathbf{V}^{-1} \mathbf{T}^\top \mathbf{V}$ is the volume-weighted adjoint of the transport matrix that gov-
 774 erns the time-reversed adjoint flow .

775 Directly analogous to Eq. (2), one can derive a relationship among $\mathbf{O}_2^{\text{pre}}$, $\mathbf{L} \mathbf{O}_2$, and
 776 $\boldsymbol{\Gamma}_\Omega^\uparrow$. Just like \mathbf{OUR} is the source term for \mathbf{TOU} , the equation for preformed oxygen shows
 777 that $\mathbf{L} \mathbf{O}_2$ is the effective source term for $\mathbf{O}_2^{\text{pre}}$. In the derivation, we can thus essentially
 778 replace \mathbf{OUR} with $\mathbf{L} \mathbf{O}_2$ and \mathbf{TOU} with $\mathbf{O}_2^{\text{pre}}$ in the matrix form of Eq. (2) to obtain
 779 $\boldsymbol{\Omega}^\top \mathbf{V} \mathbf{O}_2^{\text{pre}} = \mathbf{O}_2^\top \mathbf{L} \mathbf{V} \boldsymbol{\Gamma}_\Omega^\uparrow$. This relationship provides a direct connection between the
 780 $\mathbf{O}_2^{\text{pre}}$ inventory of Ω and the flux of $\boldsymbol{\Gamma}_\Omega^\uparrow$ into the euphotic zone. (We note in passing that
 781 this link stems from the equivalence between mixing ratio propagated forward in time
 782 from a boundary condition and the flux into that boundary from a unit-injected mass
 783 propagated in the time-reversed adjoint flow (e.g., Holzer & Hall, 2000).) The relation-
 784 ship becomes clearer when recast in the forward flow in terms of the per-unit-area ven-
 785 tilation volume $\mathcal{V}_\Omega^\downarrow$, which obeys $\mathcal{V}_\Omega^\downarrow = \mathbf{A}^{-1} \mathbf{L} \mathbf{V} \boldsymbol{\Gamma}_\Omega^\uparrow$, where \mathbf{A} is a diagonal matrix with
 786 the horizontal area of each grid cell along the diagonal. The $\mathbf{O}_2^{\text{pre}}$ inventory of Ω is thus
 787 equal to $\mathbf{O}_2^\top \mathbf{A} \mathcal{V}_\Omega^\downarrow$, which is the matrix form of Eq. (4). One could also write it as $\mathbf{O}_2^\top \mathbf{V} \mathbf{f}_\Omega^\downarrow$
 788 where $\mathbf{f}_\Omega^\downarrow$ is the vector of the fractional Ω volume ventilated by each euphotic-zone grid
 789 cell used in the work of Fu et al. (2018).

790 **Appendix C TOU and O_2^{pre} : patterns and drivers**

791 The left plots of Fig. C1 show the Pacific zonal mean O_2^{pre} for the preindustrial state
 792 and the corresponding future changes. Near the surface, O_2^{pre} is higher in cold waters
 793 with greater oxygen solubility, and in the interior O_2 traces out (water) ventilation path-
 794 ways. In the future states, preformed O_2 declines almost everywhere and more strongly
 795 at depth, except in the surface Southern Ocean above ~ 200 m.

796 The right plots of Fig. C1 show zonal mean TOU, which increases progressively as
 797 water traverses sinking organic matter where respiration strips out oxygen. TOU is gen-
 798 erally largest at depths of about 500–1500 m in the preindustrial state, and increases sig-
 799 nificantly at depth in the future states. TOU and its future changes are governed by both
 800 oxygen utilization rates (OUR) and upstream sweeping times, shown below.

801 OUR, shown in the left plots of Fig. C2, is generally surface intensified by several
 802 orders of magnitude as OUR is tightly linked to nutrient and carbon remineralization
 803 which attenuates quickly with depth. In our future states, biological production and OUR
 804 decline globally though there are some local increases, mostly owing to spatial shifts in
 805 the nutrient supply. However, the effect of changes in OUR on O_2 is modulated by the
 806 time over which oxygen is exposed to respiration, discussed next.

807 The zonal-mean upstream exposure time $\Gamma_\Omega^\uparrow(\mathbf{r})$ is shown in Fig. C2 for the case where
 808 the interior volume Ω of interest is either the upper ETP (middle plots) or deep ETP
 809 (right plots). Because in steady state $\Gamma_\Omega^\uparrow(\mathbf{r})$ is also the time that water at \mathbf{r} will spend
 810 in Ω , its magnitude approximately scales with the volume of Ω . Furthermore, because
 811 the deep circulation is much more sluggish than in the wind-driven thermocline, upstream
 812 exposure times are shorter for the upper ETP (less than ~ 20 years) than for the deep
 813 ETP (up to ~ 450 years). Γ_Ω^\uparrow is generally larger close to Ω and decreases with distance
 814 from Ω . Qualitatively, Γ_Ω^\uparrow can be thought of as path selector roughly akin to the con-
 815 centration of fluid elements destined to pass through Ω before exposure to the euphotic
 816 zone. Thus, Γ_Ω^\uparrow is shorter further away from Ω because more of the water there will be
 817 reexposed to the euphotic zone before it has a chance to pass through Ω .

818 In the future states, a slower circulation tends to increase Γ_Ω^\uparrow , but altered venti-
 819 lation pathways can also reduce Γ_Ω^\uparrow (lower middle and right plots of Fig. C2). For the
 820 deep ETP, the circulation slowdown drives strong Γ_Ω^\uparrow increases throughout the deep Pa-

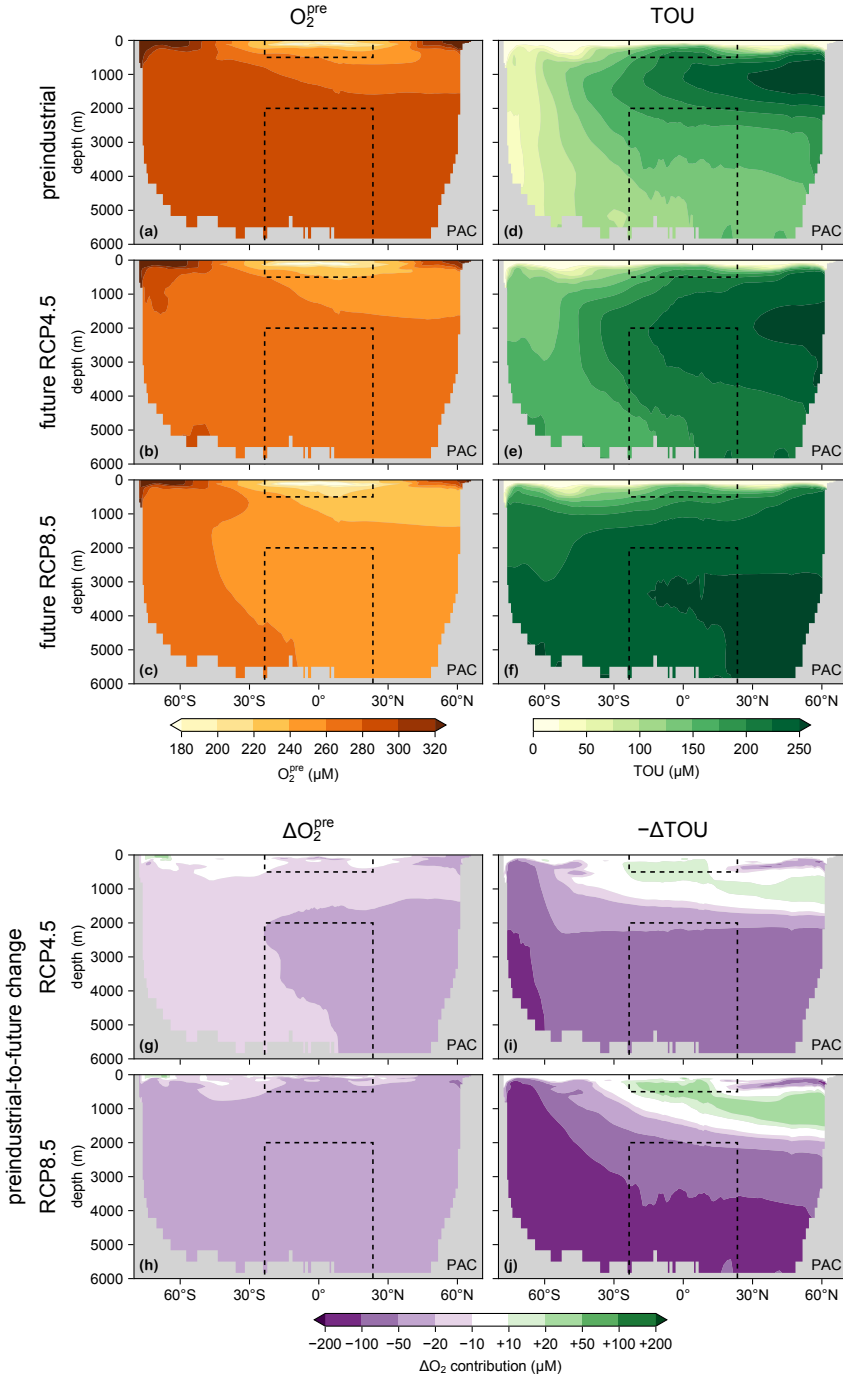


Figure C1. (a) Pacific zonal mean O_2^{pre} for the preindustrial state. (b–c) As (a) for the future states (based on RCP4.5 and RCP8.5). (d–f) As (a–c) for TOU. (g–j) ΔO_2^{pre} and ΔTOU for RCP4.5 and RCP8.5. Dashed lines indicate the upper and deep ETP regions. Note the nonlinear color scale and that the Sea of Japan has been excluded so that these zonal means are more cleanly interpretable.

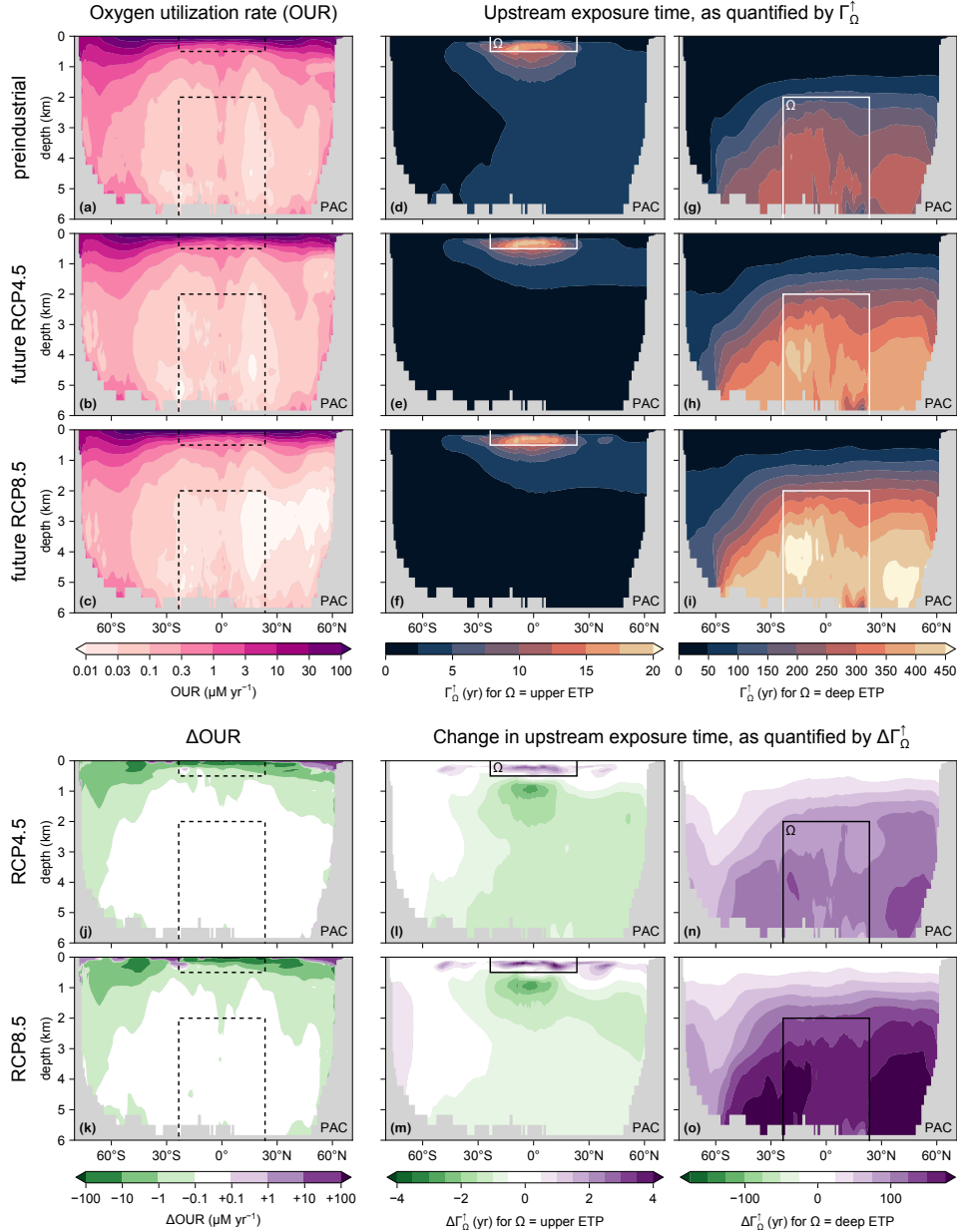


Figure C2. (a) Pacific zonal mean OUR for the preindustrial state. Dashed lines indicate the upper and deep ETP regions (Ω 's). (b–c) As (a) for the future states (RCP4.5 and RCP8.5). (d–f) As (a–c) for the upstream exposure time Γ_Ω^\uparrow of the upper ETP (above 500 m; solid white line). (g–i) As (d–f) for the deep ETP (below 2000 m). (j–k) As (b–c) for ΔOUR . (l,m,n,o) As (e,f,h,i) for $\Delta\Gamma_\Omega^\uparrow$. Note the nonlinear color scales and that the Sea of Japan has been excluded so that these zonal means are more cleanly interpretable.

cific north of the Southern Ocean. By contrast, for the upper ETP, Γ_Ω^\uparrow increases above 500 m, but decreases in the Pacific below the thermocline north of $\sim 30^\circ\text{S}$. These decreases

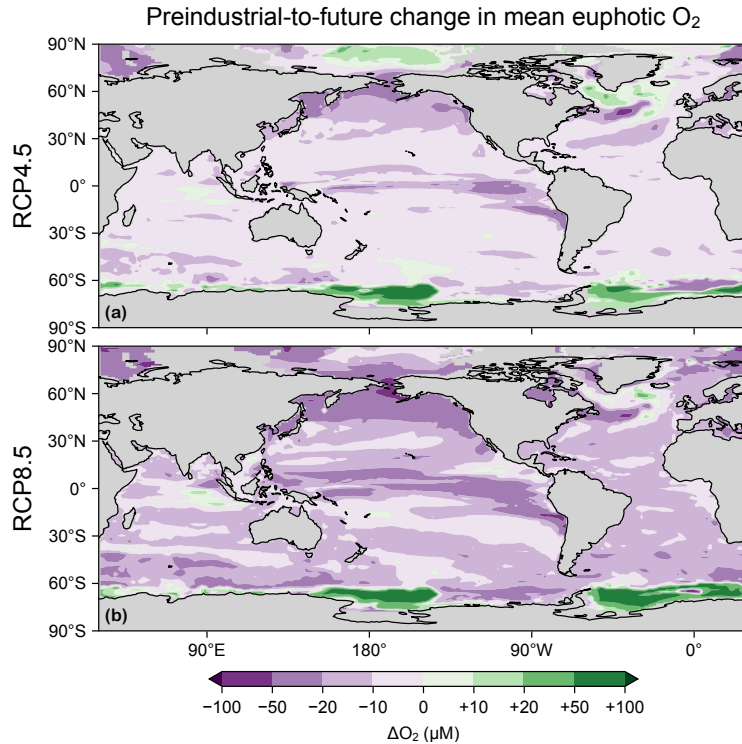


Figure C3. (a) Preindustrial-to-future change in the euphotic-mean O_2 for the RCP4.5-based scenario. (b) As (a) for RCP8.5. Note the nonlinear color scale.

are likely because the surface ocean becomes more isolated in the future (Pasquier, Holzer, & Chamberlain, 2023), reducing the flow of mid-depth, low-latitude waters through the upper ETP on their way back to the surface. Conversely, slight increases in $\Gamma_{\Omega}^{\uparrow}$ in the deep polar Southern Ocean for RCP8.5 are likely due to deep Southern Ocean waters preferentially upwelling at low latitudes in the future instead of being quickly mixed back to the Southern Ocean euphotic zone.

Changes in O_2^{pre} are driven by changes in euphotic O_2 and by changes in ventilation patterns. Fig. C3 shows maps of the changes in euphotic-mean oxygen concentrations. Except at high latitudes, declines are widespread and attributable to warming-driven solubility reductions. Increases can be caused by decreased temperatures (e.g., in the North Atlantic cold blob) but the most intense increases occur near the Weddell and Ross Seas due to reduced vertical mixing, which allows for better air-sea oxygen equilibration as discussed in Section 3.2 of the main text. However, solubility changes are not the dominant driver of reduced interior O_2^{pre} concentrations.

Decreases in the O_2^{pre} inventory of an interior subvolume Ω are dominantly driven by changes in ventilation patterns (Section 3.2), as quantified by the amount of the Ω volume ventilated per unit area, $\mathcal{V}_\Omega^\downarrow$. Maps of $\mathcal{V}_\Omega^\downarrow$ for Ω being the upper and deep ETP are plotted in Fig. C4 for the preindustrial state, along with the future changes. The patterns of $\mathcal{V}_\Omega^\downarrow$ strongly mirror those of $O_2 \mathcal{V}_\Omega^\downarrow$ in Fig. 8 of the main text. While $\sim 40\%$ of the upper ETP is ventilated from directly above, the remaining $\sim 60\%$ is ventilated from distant regions, with subtropical and subpolar contributions in the Pacific, as well as contributions from the North Atlantic, the Ross Sea, and the Weddell Sea. By contrast, the bulk of the deep ETP is ventilated from distant regions, with only about 1% from directly above. In our future states, the subpolar and Southern Ocean contributions generally decline in favor of subtropical and tropical contributions, effectively shifting the origin of preformed O_2 equatorward where warmer waters hold less dissolved oxygen.

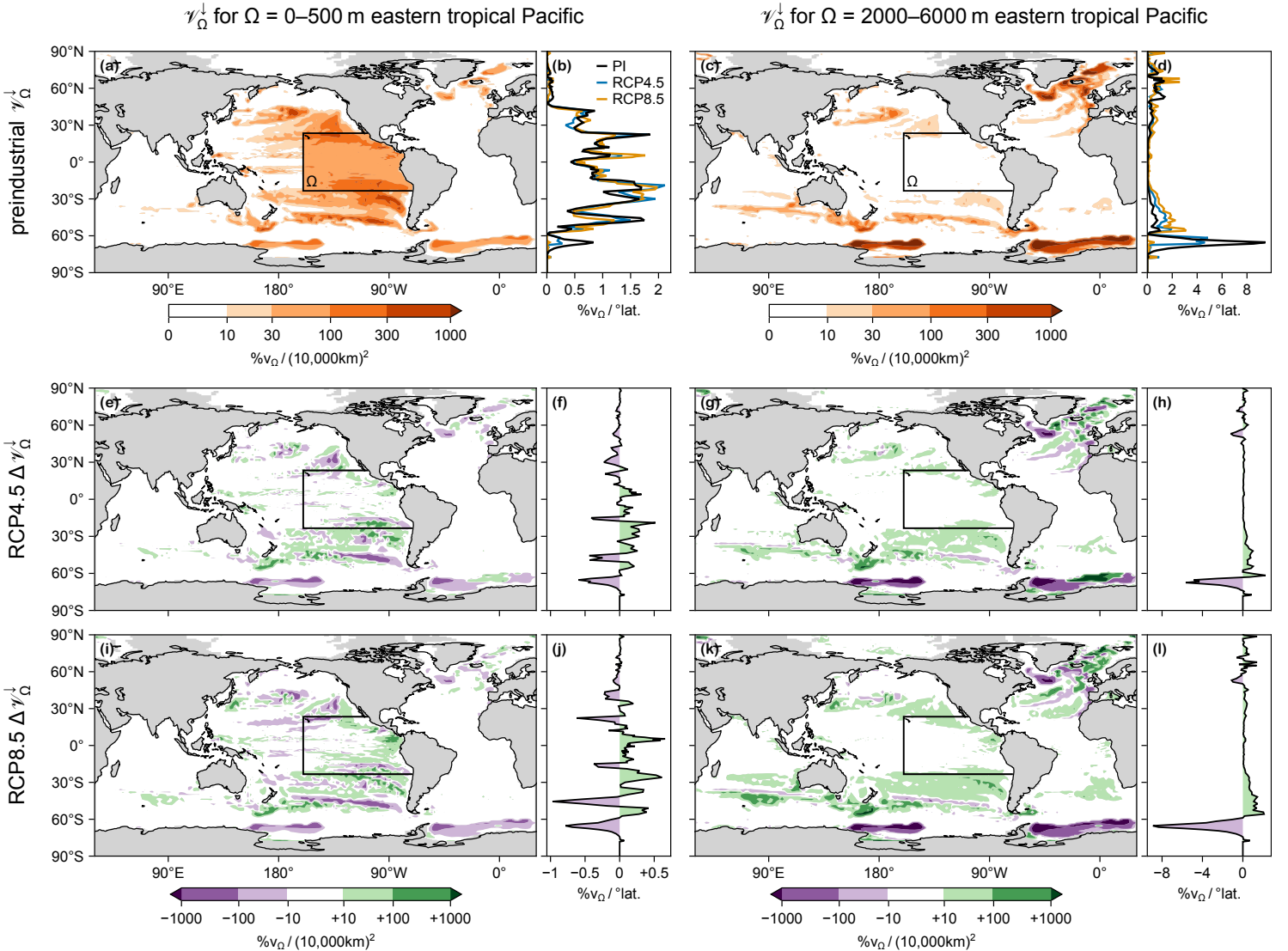


Figure C4. (a) Map and (b) zonal integral of the fractional Ω volume ventilated from the surface for Ω being the upper ETP (solid black contour), as quantified by γ_Ω^\downarrow , in the preindustrial state. (c–d) As (a–b) for Ω being the deep ETP. (e–h) As (a–d) for $\Delta\gamma_\Omega^\downarrow$ in the RCP4.5 scenario. (i–l) As (e–h) in the RCP8.5 scenario. Note the nonlinear color scales.

849 **Appendix D Open Research**

850 The MATLAB and Julia code corresponding to this work will be made available
 851 upon acceptance of this article. The figures were created in Julia (Bezanson et al., 2017)
 852 with the Makie.jl plotting package (Danisch & Krumbiegel, 2021). The transport ma-
 853 trices were built from the historical, RCP4.5, and RCP8.5 ACCESS1.3 CMIP5 model
 854 runs available at <https://esgf.nci.org.au/projects/esgfnici/>. This output also in-
 855 cludes temperature, salinity, photosynthetically available radiation (PAR), sea-ice, and
 856 wind fields.

857 **Acknowledgments**

858 This work was supported by Australian Research Council grant DP210101650 (to
 859 MH) and undertaken with the assistance of resources and services from the National Com-
 860 putational Infrastructure (NCI), which is supported by the Australian Government. NLB
 861 support for this project received grant funding from the Australian Government as part
 862 of the Antarctic Science Collaboration Initiative program.

863 **References**

- 864 Arias, P., Bellouin, N., Coppola, E., Jones, R., Krinner, G., Marotzke, J., ... Zick-
 865 feld, K. (2021). Technical summary [Book Section]. In V. Masson-Delmotte
 866 et al. (Eds.), *Climate change 2021: The physical science basis. contribution of*
 867 *working group i to the sixth assessment report of the intergovernmental panel*
 868 *on climate change* (pp. 33–144). Cambridge, United Kingdom and New York,
 869 NY, USA: Cambridge University Press. doi: 10.1017/9781009157896.002
- 870 Bao, Y., & Li, Y. (2016, December). Simulations of dissolved oxygen concentration
 871 in CMIP5 Earth system models. *Acta Oceanologica Sinica*, 35(12), 28–37. doi:
 872 10.1007/s13131-016-0959-x
- 873 Beman, J. M., & Carolan, M. T. (2013). Deoxygenation alters bacterial diversity
 874 and community composition in the ocean's largest oxygen minimum zone. *Na-*
 875 *ture Communications*, 4(1), 2705. doi: 10.1038/ncomms3705
- 876 Bezanson, J., Edelman, A., Karpinski, S., & Shah, V. B. (2017). Julia: A fresh ap-
 877 proach to numerical computing. *SIAM Review*, 59(1), 65–98. doi: 10.1137/
 878 141000671

- 879 Bi, D., Marsland, S. J., Uotila, P., O'Farrell, S., Fiedler, R. A. S., Sullivan, A., ...
 880 Hirst, A. C. (2013). ACCESS-OM: the ocean and sea ice core of the ACCESS
 881 coupled model. *Australian Meteorological and Oceanographic Journal*, 63,
 882 213-232.
- 883 Bindoff, N. L., Cheung, W. W. L., Kairo, J. G., Arístegui, J., Guinder, V. A.,
 884 Hallberg, R., ... Williamson, P. (2022). Changing Ocean, Marine Ecosys-
 885 tems, and Dependent Communities. In *The Ocean and Cryosphere in a*
 886 *Changing Climate: Special Report of the Intergovernmental Panel on Cli-*
 887 *mate Change* (pp. 447–588). Cambridge: Cambridge University Press. doi:
 888 10.1017/9781009157964.007
- 889 Bopp, L., Le Quéré, C., Heimann, M., Manning, A. C., & Monfray, P. (2002).
 890 Climate-induced oceanic oxygen fluxes: Implications for the contempo-
 891 rary carbon budget. *Global Biogeochemical Cycles*, 16(2), 6-1-6-13. doi:
 892 10.1029/2001GB001445
- 893 Bopp, L., Resplandy, L., Orr, J. C., Doney, S. C., Dunne, J. P., Gehlen, M., ...
 894 Vichi, M. (2013). Multiple stressors of ocean ecosystems in the 21st century:
 895 Projections with CMIP5 models. *Biogeosciences*, 10(10), 6225–6245. doi:
 896 10.5194/bg-10-6225-2013
- 897 Bopp, L., Resplandy, L., Untersee, A., Le Mezo, P., & Kageyama, M. (2017). Ocean
 898 (de)oxygenation from the Last Glacial Maximum to the twenty-first cen-
 899 tury: Insights from Earth System models. *Philosophical Transactions of the*
 900 *Royal Society A: Mathematical, Physical and Engineering Sciences*, 375(2102),
 901 20160323. doi: 10.1098/rsta.2016.0323
- 902 Brandt, P., Bange, H. W., Banyte, D., Dengler, M., Didwischus, S.-H., Fischer, T.,
 903 ... Visbeck, M. (2015). On the role of circulation and mixing in the venti-
 904 lation of oxygen minimum zones with a focus on the eastern tropical North
 905 Atlantic. *Biogeosciences*, 12(2), 489–512. doi: 10.5194/bg-12-489-2015
- 906 Breitburg, D., Levin, L. A., Oschlies, A., Grégoire, M., Chavez, F. P., Conley, D. J.,
 907 ... Zhang, J. (2018). Declining oxygen in the global ocean and coastal waters.
 908 *Science*, 359(6371), eaam7240. doi: 10.1126/science.aam7240
- 909 Broecker, W. S., & Peng, T.-H. (1982). Tracers in the Sea. *Lamont-Doherty Geolog-*
 910 *ical Observatory, Columbia University Palisades, New York*, 24(3), b1-b2. doi:
 911 10.1017/S0033822200005221

- 912 Buchanan, P. J., & Tagliabue, A. (2021). The Regional Importance of Oxygen De-
913 mand and Supply for Historical Ocean Oxygen Trends. *Geophysical Research
Letters*, 48(20), e2021GL094797. doi: 10.1029/2021GL094797
- 914
- 915 Busecke, J. J. M., Resplandy, L., Ditkovsky, S. J., & John, J. G. (2022). Diverging
916 Fates of the Pacific Ocean Oxygen Minimum Zone and Its Core in a Warming
917 World. *AGU Advances*, 3(6), e2021AV000470. doi: 10.1029/2021AV000470
- 918 Chamberlain, M. A., Matear, R. J., Holzer, M., Bi, D., & Marsland, S. J. (2019).
919 Transport matrices from standard ocean-model output and quantifying cir-
920 culation response to climate change. *Ocean Modelling*, 135, 1-13. doi:
921 10.1016/j.ocemod.2019.01.005
- 922 Cheng, L., von Schuckmann, K., Abraham, J. P., Trenberth, K. E., Mann, M. E.,
923 Zanna, L., ... Lin, X. (2022). Past and future ocean warming. *Nature Reviews
Earth & Environment*, 3(11), 776–794. doi: 10.1038/s43017-022-00345-1
- 924
- 925 Cliff, E., Khatiwala, S., & Schmittner, A. (2021). Glacial deep ocean deoxygena-
926 tion driven by biologically mediated air-sea disequilibrium. *Nature Geoscience*,
927 14(1), 43–50. doi: 10.1038/s41561-020-00667-z
- 928 Couespel, D., Lévy, M., & Bopp, L. (2019). Major Contribution of Reduced
929 Upper Ocean Oxygen Mixing to Global Ocean Deoxygenation in an Earth
930 System Model. *Geophysical Research Letters*, 46(21), 12239–12249. doi:
931 10.1029/2019GL084162
- 932 Danisch, S., & Krumbiegel, J. (2021). Makie.jl: Flexible high-performance data vi-
933 sualization for Julia. *Journal of Open Source Software*, 6(65), 3349. doi: 10
934 .21105/joss.03349
- 935 de Lavergne, C., Palter, J. B., Galbraith, E. D., Bernardello, R., & Marinov, I.
936 (2014). Cessation of deep convection in the open Southern Ocean under an-
937 thropogenic climate change. *Nature Climate Change*, 4(4), 278–282. doi:
938 10.1038/nclimate2132
- 939 Deutsch, C., Emerson, S., & Thompson, L. (2006). Physical-biological interactions
940 in North Pacific oxygen variability. *Journal of Geophysical Research: Oceans*,
941 111(C9). doi: 10.1029/2005JC003179
- 942 Deutsch, C., Ferrel, A., Seibel, B., Pörtner, H.-O., & Huey, R. B. (2015). Climate
943 change tightens a metabolic constraint on marine habitats. *Science*, 348(6239),
944 1132–1135. doi: 10.1126/science.aaa1605

- 945 Deutsch, C., Penn, J. L., & Lucey, N. (2024). Climate, Oxygen, and the Future of
 946 Marine Biodiversity. *Annual Review of Marine Science*, 16(1), null. doi: 10
 947 .1146/annurev-marine-040323-095231
- 948 DeVries, T., & Deutsch, C. (2014). Large-scale variations in the stoichiometry of
 949 marine organic matter respiration. *Nature Geoscience*, 7, 890–894. doi: 10
 950 .1038/NGEO2300
- 951 Diaz, R. J., & Rosenberg, R. (2008). Spreading Dead Zones and Consequences
 952 for Marine Ecosystems. *Science*, 321(5891), 926–929. doi: 10.1126/science
 953 .1156401
- 954 Doney, S. C., & Bullister, J. L. (1992). A chlorofluorocarbon section in the eastern
 955 North Atlantic. *Deep Sea Research Part A. Oceanographic Research Papers*,
 956 39(11), 1857–1883. doi: 10.1016/0198-0149(92)90003-C
- 957 Duteil, O., Koeve, W., Oschlies, A., Bianchi, D., Galbraith, E., Kriest, I., & Matear,
 958 R. (2013). A novel estimate of ocean oxygen utilisation points to a reduced
 959 rate of respiration in the ocean interior. *Biogeosciences*, 10(11), 7723–7738.
 960 doi: 10.5194/bg-10-7723-2013
- 961 Earle, S. A., Wright, D. J., Joye, S., Laffoley, D., Baxter, J., Safina, C., & Elkus, P.
 962 (2018, March). Ocean deoxygenation: Time for action. *Science*, 359(6383),
 963 1475–1476. doi: 10.1126/science.aat0167
- 964 Eggleston, S., & Galbraith, E. D. (2018). The devil's in the disequilibrium: Multi-
 965 component analysis of dissolved carbon and oxygen changes under a broad
 966 range of forcings in a general circulation model. *Biogeosciences*, 15(12), 3761–
 967 3777. doi: 10.5194/bg-15-3761-2018
- 968 Ekau, W., Auel, H., Pörtner, H.-O., & Gilbert, D. (2010). Impacts of hy-
 969 poxia on the structure and processes in pelagic communities (zooplank-
 970 ton, macro-invertebrates and fish). *Biogeosciences*, 7(5), 1669–1699. doi:
 971 10.5194/bg-7-1669-2010
- 972 Espinoza-Morriberón, D., Echevin, V., Gutiérrez, D., Tam, J., Graco, M., Ledesma,
 973 J., & Colas, F. (2021). Evidences and drivers of ocean deoxygenation
 974 off Peru over recent past decades. *Scientific Reports*, 11(1), 20292. doi:
 975 10.1038/s41598-021-99876-8
- 976 Falkowski, P. G., & Godfrey, L. V. (2008). Electrons, life and the evolution of
 977 Earth's oxygen cycle. *Philosophical Transactions of the Royal Society B:*

- 978 *Biological Sciences*, 363(1504), 2705–2716. doi: 10.1098/rstb.2008.0054
- 979 Feely, R. A., Sabine, C. L., Schlitzer, R., Bullister, J. L., Mecking, S., & Greeley, D.
- 980 (2004). Oxygen Utilization and Organic Carbon Remineralization in the Upper
- 981 Water Column of the Pacific Ocean. *Journal of Oceanography*, 60(1), 45–52.
- 982 doi: 10.1023/B:JOCE.0000038317.01279.aa
- 983 Franco, A. C., Kim, H., Frenzel, H., Deutsch, C., Ianson, D., Sumaila, U. R., &
- 984 Tortell, P. D. (2022). Impact of warming and deoxygenation on the habitat
- 985 distribution of Pacific halibut in the Northeast Pacific. *Fisheries Oceanogra-*
- 986 phy, 31(6), 601–614. doi: 10.1111/fog.12610
- 987 Frölicher, T. L., Aschwanden, M. T., Gruber, N., Jaccard, S. L., Dunne, J. P.,
- 988 & Paynter, D. (2020). Contrasting Upper and Deep Ocean Oxygen Re-
- 989 sponse to Protracted Global Warming. *Global Biogeochemical Cycles*, 34(8),
- 990 e2020GB006601. doi: 10.1029/2020GB006601
- 991 Fu, W., Bardin, A., & Primeau, F. W. (2018). Tracing ventilation source of tropical
- 992 pacific oxygen minimum zones with an adjoint global ocean transport model.
- 993 *Deep Sea Research Part I: Oceanographic Research Papers*, 139, 95–103. doi:
- 994 10.1016/j.dsr.2018.07.017
- 995 Gallo, N. D., & Levin, L. A. (2016). Chapter Three - Fish Ecology and Evolution
- 996 in the World's Oxygen Minimum Zones and Implications of Ocean Deoxygenation.
- 997 In B. E. Curry (Ed.), *Advances in Marine Biology* (Vol. 74, pp. 117–198).
- 998 Academic Press. doi: 10.1016/bs.amb.2016.04.001
- 999 Gnanadesikan, A., Dunne, J. P., & John, J. (2012). Understanding why the
- 1000 volume of suboxic waters does not increase over centuries of global warm-
- 1001 ing in an Earth System Model. *Biogeosciences*, 9(3), 1159–1172. doi:
- 1002 10.5194/bg-9-1159-2012
- 1003 Graco, M. I., Purca, S., Dewitte, B., Castro, C. G., Morón, O., Ledesma, J., ...
- 1004 Gutiérrez, D. (2017). The OMZ and nutrient features as a signature of in-
- 1005 terannual and low-frequency variability in the Peruvian upwelling system.
- 1006 *Biogeosciences*, 14(20), 4601–4617. doi: 10.5194/bg-14-4601-2017
- 1007 Gunn, K. L., Rintoul, S. R., England, M. H., & Bowen, M. M. (2023). Recent re-
- 1008 duced abyssal overturning and ventilation in the Australian Antarctic Basin.
- 1009 *Nature Climate Change*, 13(6), 537–544. doi: 10.1038/s41558-023-01667-8
- 1010 Helm, K. P., Bindoff, N. L., & Church, J. A. (2011). Observed decreases in oxy-

- 1011 gen content of the global ocean. *Geophysical Research Letters*, 38(23). doi: 10
1012 .1029/2011GL049513
- 1013 Heuzé, C., Heywood, K. J., Stevens, D. P., & Ridley, J. K. (2013). Southern Ocean
1014 bottom water characteristics in CMIP5 models. *Geophysical Research Letters*,
1015 40(7), 1409–1414. doi: 10.1002/grl.50287
- 1016 Hofmann, A. F., Peltzer, E. T., Walz, P. M., & Brewer, P. G. (2011). Hypoxia by
1017 degrees: Establishing definitions for a changing ocean. *Deep Sea Research Part*
1018 *I: Oceanographic Research Papers*, 58(12), 1212–1226. doi: 10.1016/j.dsr.2011
1019 .09.004
- 1020 Holzer, M. (2022). The fate of oxygen in the ocean and its sensitivity to lo-
1021 cal changes in biological production. *Journal of Geophysical Research: Oceans*, 127(8), e2022JC018802.
1022 (e2022JC018802 2022JC018802) doi:
1023 10.1029/2022JC018802
- 1024 Holzer, M., Chamberlain, M. A., & Matear, R. J. (2020). Climate-driven changes
1025 in the ocean's ventilation pathways and time scales diagnosed from transport
1026 matrices. *Journal of Geophysical Research: Oceans*, 125(10), e2020JC016414.
1027 (e2020JC016414 10.1029/2020JC016414) doi: 10.1029/2020JC016414
- 1028 Holzer, M., DeVries, T., & de Lavergne, C. (2021). Diffusion controls the ventilation
1029 of a Pacific Shadow Zone above abyssal overturning. *Nature Communications*,
1030 12(1), 4348. doi: 10.1038/s41467-021-24648-x
- 1031 Holzer, M., & Hall, T. M. (2000). Transit-Time and Tracer-Age Distributions in
1032 Geophysical Flows. *Journal of the Atmospheric Sciences*, 57(21), 3539–3558.
1033 doi: 10.1175/1520-0469(2000)057<3539:TTATAD>2.0.CO;2
- 1034 Ito, T., Follows, M. J., & Boyle, E. A. (2004). Is AOU a good measure of respi-
1035 ration in the oceans? *Geophysical Research Letters*, 31(17). doi: 10.1029/
1036 2004GL020900
- 1037 Ito, T., Takano, Y., Deutsch, C., & Long, M. C. (2022). Sensitivity of Global
1038 Ocean Deoxygenation to Vertical and Isopycnal Mixing in an Ocean Biogeo-
1039 chemistry Model. *Global Biogeochemical Cycles*, 36(4), e2021GB007151. doi:
1040 10.1029/2021GB007151
- 1041 Jin, X., Najjar, R. G., Louanchi, F., & Doney, S. C. (2007). A modeling study of the
1042 seasonal oxygen budget of the global ocean. *Journal of Geophysical Research:*
1043 *Oceans*, 112(C5). doi: 10.1029/2006JC003731

- 1044 Keeling, R. F., & Garcia, H. E. (2002). The change in oceanic O₂ inventory associated
 1045 with recent global warming. *Proceedings of the National Academy of Sciences*, 99(12), 7848–7853. doi: 10.1073/pnas.122154899
- 1046
- 1047 Keeling, R. F., Körtzinger, A., & Gruber, N. (2010). Ocean Deoxygenation in a
 1048 Warming World. *Annual Review of Marine Science*, 2(1), 199–229. doi: 10
 1049 .1146/annurev.marine.010908.163855
- 1050 Koeve, W., & Kähler, P. (2016). Oxygen utilization rate (OUR) underestimates
 1051 ocean respiration: A model study. *Global Biogeochemical Cycles*, 30(8), 1166–
 1052 1182. doi: 10.1002/2015GB005354
- 1053 Kwiatkowski, L., Torres, O., Bopp, L., Aumont, O., Chamberlain, M., Christian,
 1054 J. R., ... Ziehn, T. (2020). Twenty-first century ocean warming, acidification,
 1055 deoxygenation, and upper-ocean nutrient and primary production decline
 1056 from CMIP6 model projections. *Biogeosciences*, 17(13), 3439–3470. doi:
 1057 10.5194/bg-17-3439-2020
- 1058 Laffoley, D., & Baxter, J. M. (2019). *Ocean deoxygenation: Everyone's problem:
 1059 Causes, impacts, consequences and solutions: Summary for Policy Makers* (Report). Gland: International Union for Conservation of Nature (IUCN). doi:
 1060 10.2305/IUCN.CH.2019.14.en
- 1061
- 1062 Lauvset, S. K., Key, R. M., Olsen, A., van Heuven, S., Velo, A., Lin, X., ... Wa-
 1063 teleit, S. (2016). A new global interior ocean mapped climatology: The
 1064 1 × 1 GLODAP version 2. *Earth System Science Data*, 8(2), 325–340. doi:
 1065 10.5194/essd-8-325-2016
- 1066 Levin, L. A. (2018). Manifestation, Drivers, and Emergence of Open Ocean De-
 1067 oxygennation. *Annual Review of Marine Science*, 10, 229–260. doi: 10.1146/
 1068 annurev-marine-121916-063359
- 1069 Li, Q., England, M. H., Hogg, A. M., Rintoul, S. R., & Morrison, A. K. (2023).
 1070 Abyssal ocean overturning slowdown and warming driven by Antarctic meltwa-
 1071 ter. *Nature*, 615(7954), 841–847. doi: 10.1038/s41586-023-05762-w
- 1072 Long, M. C., Ito, T., & Deutsch, C. (2019). Oxygen projections for the future. In
 1073 *Ocean deoxygenation: Everyone's problem — causes, impacts, consequences
 1074 and solutions* (pp. 171–211). Gland, Switzerland: IUCN.
- 1075 Marsland, S., Bi, D., Uotila, P., Fiedler, R., Griffies, S., Lorbacher, K., ... Hirst,
 1076 A. (2013). Configuration and spin-up of ACCESS-CM2, the new genera-

- 1077 Australian Community Climate and Earth System Simulator Coupled
1078 Model. *Australian Meteorological and Oceanographic Journal*, 63, 101–119.
1079 doi: 10.22499/2.6301.007

1080 Matear, R. J., & Hirst, A. C. (2003). Long-term changes in dissolved oxygen concen-
1081 trations in the ocean caused by protracted global warming. *Global Biogeochemical Cycles*, 17(4). doi: 10.1029/2002GB001997
1082

1083 Matear, R. J., Hirst, A. C., & McNeil, B. I. (2000). Changes in dissolved oxygen in
1084 the Southern Ocean with climate change. *Geochemistry, Geophysics, Geosys-
1085 tems*, 1(11). doi: 10.1029/2000GC000086

1086 McCormick, L. R., & Levin, L. A. (2017). Physiological and ecological implica-
1087 tions of ocean deoxygenation for vision in marine organisms. *Philosophical
1088 Transactions of the Royal Society A: Mathematical, Physical and Engineering
1089 Sciences*, 375(2102), 20160322. doi: 10.1098/rsta.2016.0322

1090 McCormick, L. R., Levin, L. A., & Oesch, N. W. (2019). Vision is highly sensitive to
1091 oxygen availability in marine invertebrate larvae. *Journal of Experimental Bi-
1092 ology*, 222(10), jeb200899. doi: 10.1242/jeb.200899

1093 Meinshausen, M., Nicholls, Z. R. J., Lewis, J., Gidden, M. J., Vogel, E., Freund, M.,
1094 ... Wang, R. H. J. (2020). The shared socio-economic pathway (ssp) green-
1095 house gas concentrations and their extensions to 2500. *Geoscientific Model
1096 Development*, 13(8), 3571–3605. doi: 10.5194/gmd-13-3571-2020

1097 Meinshausen, M., Smith, S. J., Calvin, K., Daniel, J. S., Kainuma, M. L. T., Lamar-
1098 que, J.-F., ... van Vuuren, D. P. (2011). The RCP greenhouse gas concentra-
1099 tions and their extensions from 1765 to 2300. *Climatic Change*, 109(1), 213.
1100 doi: 10.1007/s10584-011-0156-z

1101 Mongwe, P., Long, M., Ito, T., Deutsch, C., & Santana-Falcón, Y. (under review).
1102 Climatic Controls on Metabolic Constraints in the Ocean. *EGUsphere*, 1–29.
1103 doi: 10.5194/egusphere-2023-2822

1104 Moore, J. K., Fu, W., Primeau, F. W., Britten, G. L., Lindsay, K., Long, M.,
1105 ... Randerson, J. T. (2018). Sustained climate warming drives declin-
1106 ing marine biological productivity. *Science*, 359(6380), 1139–1143. doi:
1107 10.1126/science.aa06379

1108 Morée, A. L., Clarke, T. M., Cheung, W. W. L., & Frölicher, T. L. (2023). Impact of
1109 deoxygenation and warming on global marine species in the 21st century. *Bio-*

- 1110 *geosciences*, 20(12), 2425–2454. doi: 10.5194/bg-20-2425-2023
- 1111 Oschlies, A. (2021). A committed fourfold increase in ocean oxygen loss. *Nature Communications*, 12(1), 2307. doi: 10.1038/s41467-021-22584-4
- 1112 Oschlies, A., Brandt, P., Stramma, L., & Schmidtko, S. (2018). Drivers and mechanisms of ocean deoxygenation. *Nature Geoscience*, 11(7), 467–473. doi: 10.1038/s41561-018-0152-2
- 1113 Oschlies, A., Koeve, W., Landolfi, A., & Kähler, P. (2019). Loss of fixed nitrogen causes net oxygen gain in a warmer future ocean. *Nature Communications*, 10(1), 2805. doi: 10.1038/s41467-019-10813-w
- 1114 Palter, J. B., & Trossman, D. S. (2018). The Sensitivity of Future Ocean Oxygen to Changes in Ocean Circulation. *Global Biogeochemical Cycles*, 32(5), 738–751. doi: 10.1002/2017GB005777
- 1115 Pascal, L., Cool, J., Archambault, P., Calosi, P., Cuenca, A. L. R., Mucci, A. O., & Chaillou, G. (2023). Ocean deoxygenation caused non-linear responses in the structure and functioning of benthic ecosystems. *Global Change Biology*, n/a(n/a), e16994. doi: 10.1111/gcb.16994
- 1116 Pasquier, B., Holzer, M., & Chamberlain, M. A. (2023, December). The ocean's biological and preformed carbon pumps in future steady-state climate scenarios. *EGUsphere*, 1–41. doi: 10.5194/egusphere-2023-2525
- 1117 Pasquier, B., Holzer, M., Chamberlain, M. A., Matear, R. J., Bindoff, N. L., & Primeau, F. W. (2023). Optimal parameters for the ocean's nutrient, carbon, and oxygen cycles compensate for circulation biases but replumb the biological pump. *Biogeosciences (Online)*, 20(14), 2985–3009. doi: 10.5194/bg-20-2985-2023
- 1118 Pitcher, G. C., Aguirre-Velarde, A., Breitburg, D., Cardich, J., Carstensen, J., Conley, D. J., ... Zhu, ZY. (2021). System controls of coastal and open ocean oxygen depletion. *Progress in Oceanography*, 197, 102613. doi: 10.1016/j.pocean.2021.102613
- 1119 Plattner, G.-K., Joos, F., Stocker, T. F., & Marchal, O. (2001). Feedback mechanisms and sensitivities of ocean carbon uptake under global warming. *Tellus B: Chemical and Physical Meteorology*, 53(5), 564–592. doi: 10.3402/tellusb.v53i5.16637
- 1120 Primeau, F. W. (2005). Characterizing transport between the surface mixed

- layer and the ocean interior with a forward and adjoint global ocean transport model. *Journal of Physical Oceanography*, 35(4), 545–564. doi: 10.1175/JPO2699.1
- Riahi, K., van Vuuren, D. P., Kriegler, E., Edmonds, J., O'Neill, B. C., Fujimori, S., ... Tavoni, M. (2017). The shared socioeconomic pathways and their energy, land use, and greenhouse gas emissions implications: An overview. *Global Environmental Change*, 42, 153–168. doi: 10.1016/j.gloenvcha.2016.05.009
- Roach, C. J., & Bindoff, N. L. (2023). Developing a New Oxygen Atlas of the World's Oceans Using Data Interpolating Variational Analysis. *Journal of Atmospheric and Oceanic Technology*, 40(11), 1475–1491. doi: 10.1175/JTECH-D-23-0007.1
- Rogers, A. D. (2000). The role of the oceanic oxygen minima in generating biodiversity in the deep sea. *Deep Sea Research Part II: Topical Studies in Oceanography*, 47(1), 119–148. doi: 10.1016/S0967-0645(99)00107-1
- Russell, J. L., & Dickson, A. G. (2003). Variability in oxygen and nutrients in South Pacific Antarctic Intermediate Water. *Global Biogeochemical Cycles*, 17(2). doi: 10.1029/2000GB001317
- Sarmiento, J. L., Herbert, T. D., & Toggweiler, J. R. (1988). Causes of anoxia in the world ocean. *Global Biogeochemical Cycles*, 2(2), 115–128. doi: 10.1029/GB002i002p00115
- Sato, K. N., Levin, L. A., & Schiff, K. (2017). Habitat compression and expansion of sea urchins in response to changing climate conditions on the California continental shelf and slope (1994–2013). *Deep Sea Research Part II: Topical Studies in Oceanography*, 137, 377–389. doi: 10.1016/j.dsr2.2016.08.012
- Schmidtko, S., Stramma, L., & Visbeck, M. (2017). Decline in global oceanic oxygen content during the past five decades. *Nature*, 542(7641), 335–339. doi: 10.1038/nature21399
- Schmittner, A., Oschlies, A., Matthews, H. D., & Galbraith, E. D. (2008). Future changes in climate, ocean circulation, ecosystems, and biogeochemical cycling simulated for a business-as-usual co₂ emission scenario until year 4000 ad. *Global Biogeochemical Cycles*, 22(1). doi: 10.1029/2007GB002953
- Seibel, B. A. (2011). Critical oxygen levels and metabolic suppression in oceanic oxygen minimum zones. *Journal of Experimental Biology*, 214(2), 326–336.

- 1176 doi: 10.1242/jeb.049171
- 1177 Shaffer, G., Olsen, S. M., & Pedersen, J. O. P. (2009). Long-term ocean oxygen de-
1178 pletion in response to carbon dioxide emissions from fossil fuels. *Nature Geo-
1179 science*, 2(2), 105–109. doi: 10.1038/ngeo420
- 1180 Sonnerup, R. E., Mecking, S., & Bullister, J. L. (2013). Transit time distributions
1181 and oxygen utilization rates in the Northeast Pacific Ocean from chlorofluo-
1182 rocarbons and sulfur hexafluoride. *Deep Sea Research Part I: Oceanographic
1183 Research Papers*, 72, 61–71. doi: 10.1016/j.dsr.2012.10.013
- 1184 Sonnerup, R. E., Mecking, S., Bullister, J. L., & Warner, M. J. (2015). Transit time
1185 distributions and oxygen utilization rates from chlorofluorocarbons and sulfur
1186 hexafluoride in the Southeast Pacific Ocean. *Journal of Geophysical Research:
1187 Oceans*, 120(5), 3761–3776. doi: 10.1002/2015JC010781
- 1188 Srokosz, M. A., & Bryden, H. L. (2015). Observing the Atlantic Meridional Over-
1189 turning Circulation yields a decade of inevitable surprises. *Science*, 348(6241),
1190 1255575. doi: 10.1126/science.1255575
- 1191 Stramma, L., Prince, E. D., Schmidtko, S., Luo, J., Hoolihan, J. P., Visbeck, M., ...
1192 Körtzinger, A. (2012). Expansion of oxygen minimum zones may reduce avail-
1193 able habitat for tropical pelagic fishes. *Nature Climate Change*, 2(1), 33–37.
1194 doi: 10.1038/nclimate1304
- 1195 Takano, Y., Ilyina, T., Tjiputra, J., Eddebar, Y. A., Berthet, S., Bopp, L., ...
1196 Yool, A. (2023). Simulations of ocean deoxygenation in the historical era:
1197 Insights from forced and coupled models. *Frontiers in Marine Science*, 10.
- 1198 Thomas, J. L., Waugh, D. W., & Gnanadesikan, A. (2020). Relationship between
1199 Age and Oxygen along Line W in the Northwest Atlantic Ocean. *Ocean Sci-
1200 ence Journal*, 55(2), 203–217. doi: 10.1007/s12601-020-0019-5
- 1201 Vaquer-Sunyer, R., & Duarte, C. M. (2008). Thresholds of hypoxia for marine bio-
1202 diversity. *Proceedings of the National Academy of Sciences*, 105(40), 15452–
1203 15457. doi: 10.1073/pnas.0803833105
- 1204 Wanninkhof, R. (2014). Relationship between wind speed and gas exchange over the
1205 ocean revisited. *Limnology and Oceanography: Methods*, 12(6), 351–362. doi:
1206 10.4319/lom.2014.12.351
- 1207 Warner, M. J., Bullister, J. L., Wisegarver, D. P., Gammon, R. H., & Weiss, R. F.
1208 (1996). Basin-wide distributions of chlorofluorocarbons CFC-11 and CFC-12

- 1209 in the North Pacific: 1985–1989. *Journal of Geophysical Research: Oceans*,
1210 *101*(C9), 20525–20542. doi: 10.1029/96JC01849
- 1211 Whitney, F. A., Freeland, H. J., & Robert, M. (2007). Persistently declining oxy-
1212 gen levels in the interior waters of the eastern subarctic Pacific. *Progress in*
1213 *Oceanography*, *75*(2), 179–199. doi: 10.1016/j.pocean.2007.08.007
- 1214 Wishner, K. F., Seibel, B. A., Roman, C., Deutsch, C., Outram, D., Shaw, C. T.,
1215 ... Riley, S. (2018). Ocean deoxygenation and zooplankton: Very small
1216 oxygen differences matter. *Science Advances*, *4*(12), eaau5180. doi:
1217 10.1126/sciadv.aau5180
- 1218 Wyrtki, K. (1962). The oxygen minima in relation to ocean circulation. *Deep*
1219 *Sea Research and Oceanographic Abstracts*, *9*(1), 11–23. doi: 10.1016/
1220 0011-7471(62)90243-7
- 1221 Zheng, Y., Schlosser, P., Swift, J. H., & Jones, E. P. (1997). Oxygen utilization rates
1222 in the Nansen Basin, Arctic Ocean: Implications for new production. *Deep Sea*
1223 *Research Part I: Oceanographic Research Papers*, *44*(12), 1923–1943. doi: 10
1224 .1016/S0967-0637(97)00046-0